

Transcriptome analysis and molecular signature of human retinal pigment epithelium

N.V. Strunnikova^{1,4}, A. Maminishkis^{2,4}, J.J. Barb⁵, F. Wang^{2,4}, C. Zhi^{2,4}, Y. Sergeev^{1,4}, W. Chen⁶, A.O. Edwards⁷, D. Stambolian⁸, G. Abecasis⁶, A. Swaroop^{3,4}, P.J. Munson⁵ and S.S. Miller^{2,4,*}

¹Ophthalmic Genetics & Visual Function Branch, ²Section of Epithelial and Retinal Physiology and Disease, ³Neurobiology-Neurodegeneration & Repair Laboratory and ⁴National Eye Institute/NIH, Bethesda, MD, USA, ⁵Mathematical and Statistical Computing Laboratory, Center for Information Technology/NIH, Bethesda, MD, USA, ⁶Biostatistics, School of Public Health, University of Michigan, Ann Arbor, MI, USA, ⁷Institute for Molecular Biology, University of Oregon, Eugene, OR, USA and ⁸Ophthalmology, University of Pennsylvania, Philadelphia, PA, USA

Received December 14, 2009; Revised March 3, 2010; Accepted March 30, 2010

Retinal pigment epithelium (RPE) is a polarized cell layer critical for photoreceptor function and survival. The unique physiology and relationship to the photoreceptors make the RPE a critical determinant of human vision. Therefore, we performed a global expression profiling of native and cultured human fetal and adult RPE and determined a set of highly expressed 'signature' genes by comparing the observed RPE gene profiles to the Novartis expression database (SymAtlas: <http://wombat.gnf.org/index.html>) of 78 tissues. Using stringent selection criteria of at least 10-fold higher expression in three distinct preparations, we identified 154 RPE signature genes, which were validated by qRT-PCR analysis in RPE and in an independent set of 11 tissues. Several of the highly expressed signature genes encode proteins involved in visual cycle, melanogenesis and cell adhesion and Gene ontology analysis enabled the assignment of RPE signature genes to epithelial channels and transporters (*CICN4*, *BEST1*, *SLCA20*) or matrix remodeling (*TIMP3*, *COL8A2*). Fifteen RPE signature genes were associated with known ophthalmic diseases, and 25 others were mapped to regions of disease loci. An evaluation of the RPE signature genes in a recently completed AMD genomewide association (GWA) data set revealed that *TIMP3*, *GRAMD3*, *PITPNA* and *CHRNA3* signature genes may have potential roles in AMD pathogenesis and deserve further examination. We propose that RPE signature genes are excellent candidates for retinal diseases and for physiological investigations (e.g. dopachrome tautomerase in melanogenesis). The RPE signature gene set should allow the validation of RPE-like cells derived from human embryonic or induced pluripotent stem cells for cell-based therapies of degenerative retinal diseases.

INTRODUCTION

Progressive retinal degenerative diseases, such as age-related macular degeneration (AMD) and retinitis pigmentosa (RP), are major causes of untreatable blindness and have a tremendous social and financial burden on society. As many as 30 million people worldwide are afflicted with AMD, and this diagnosis is expected to increase dramatically in the coming decades because of aging populations (1,2). AMD is an aging-associated multifactorial disease that affects the

photoreceptor-retinal pigment epithelium (RPE)–choroid interface in the macula and is caused by the interaction of genetic susceptibility factors and environment (3). The RPE is the source and the target of many retinal degenerative diseases and defects in RPE function can affect the integrity and viability of neighboring cells—primarily photoreceptors (4–6).

The RPE is a polarized monolayer of epithelial cells that separates the neural retina and the choroidal blood supply and forms a highly selective barrier fundamentally important

*To whom correspondence should be addressed at: NIH, NEI, 31 Center Drive MSC 2510, Bethesda, MD 20892-2510, USA. Tel: +1 3014516763; Fax: +1 3014515421; Email: millers@nei.nih.gov

for maintaining the health and integrity of the photoreceptors (7,8). This epithelium is derived from neural ectoderm and forms a close anatomical relationship with the photoreceptors, mimicking the neuronal–glial relationship observed in the central nervous system (CNS). In the eye, light–dark transitions and circadian rhythms modulate the RPE transport of nutrients, metabolic waste products, ions and fluid between the choroidal blood supply and the subretinal space surrounding the photoreceptor outer segments (9,10). High metabolic activity and ongoing exposure to light makes the RPE particularly vulnerable to oxidative damage. Not surprisingly, abnormalities in RPE phagocytosis of rods and cones or in the maintenance of the visual cycle can lead to retinal degeneration and photoreceptor cell death (11).

Disease processes affecting RPE/photoreceptor interaction and causing RPE dysfunction have been subjects of intense scrutiny (12–14). *In vitro* models of RPE have been derived from native and cultured human cells, from fetal and postnatal donor eyes, transformed cell lines and embryonic stem (ES) cells (14–19). Cultured human RPE can be grown in large quantities and used in biochemical and functional assays (18, 20) or transplantation studies. However, the value of cultured RPE depends on its ability to recapitulate functional and genetic characteristics of the native tissue. We have previously developed a primary human fetal RPE cell culture model that mimics the normal physiology, function and structure of native fetal and adult RPE, and thus is suitable for a wide range of studies on diseases associated with retina/RPE interactions (10,18,21–23).

The global expression profile of human RPE will be valuable for elucidating its pivotal role in retinal degenerative diseases (24). Hence, we have performed a comparative analysis of transcriptomes from human fetal and adult RPE, primary cultures and commonly used human cell lines and tissues. We report a unique ‘signature’ set of 154 genes whose expression levels distinguish RPE from other tissues or cell types. We also describe a cross-sectional analysis of RPE ‘signature’ genes against an AMD genomewide association study (GWAS) (25) with a goal of identifying candidate genes and pathways relevant to AMD. Ingenuity analysis and RetNet (www.sph.uth.tmc.edu/retnet/) were used to analyze RPE signature genes to identify novel candidate genes for RPE disease. Our study provides an important discovery tool for functional investigations of RPE/photoreceptor interaction and establishes a molecular platform to evaluate RPE cells for repair of degenerating retina.

RESULTS

Human RPE ‘gene signature’

We generated global expression profiles of native fetal and adult human RPE, and of fetal primary cultures and compared these with transcriptomes of adult transformed RPE cell lines and of other human tissues (Fig. 1). Principle component analysis (PCA) and hierarchical cluster analysis were first used to evaluate similarities or differences in gene expression between samples from primary cultures and native RPE. The hierarchical clustering dendrogram based on principal components of 30 samples demonstrates that native human

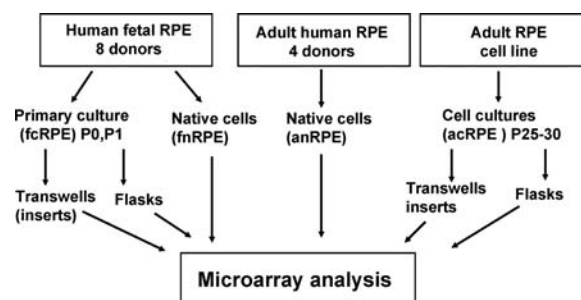


Figure 1. Experimental design. Four groups of native cells and primary RPE cultures were used for the microarray analysis (a total of 30 samples): (i) adult native RPE (AN); (ii) native fetal RPE (FN); (iii) primary cultures of fetal RPE (FC) at passage 1; (iv) ARPE-19 (AC), a transformed cell line. To determine the effect of culture conditions on gene expression of FC and AC, RPE cells were cultured on transwells or flasks. A total of 12 human donor eyes were used to collect adult and fetal native RPE cells (four donors in each case) and to establish fetal RPE primary cultures (four donors).

tissues (fnRPE and anRPE) and cultured cells (fcRPE and ARPE-19) cluster separately regardless of the sample source (Fig. 2A). In contrast, biological ($n = 4$) or technical replicates (ARPE-19; $n = 8$) in each RPE group cluster together. More than 50% of the total variability in expression data is included in PC1, PC2 and PC3 (Fig. 2B, C and see legend). Visual inspection of PC1 versus PC2 (Fig. 2B) and PC2 versus PC3 (Fig. 2C) plots reveals distinct clusters separating the four different RPE preparations.

To identify an expression profile that distinguishes human RPE from other cell types, we compared the expression of native adult and fetal RPE and primary cultures of fetal RPE against 78 different human tissues and cell cultures (26). The relative expression (rEx) values (see Materials and Methods) revealed a set of 154 highly expressed genes (171 probe sets) in anRPE, fnRPE and fcRPE (Fig. 3A and B). We call these ‘signature’ genes as they together provide a unique profile of RPE functions. Gene ontology (GO) analysis further identified several critical functional groups significantly over-represented in the ‘signature’ genes ($P < 0.005$). These include (i) vision, perception of light and vitamin A metabolism (e.g. *CRX*, *EFEMP1*, *RPE65*, *SFRP5*, *SIX3*, *TIMP3*, *BEST1*, *RDH11*, *RBP1*); (ii) response to stimulus and sensory perception (e.g. *AHR*, *CDH3*, *GJA1*, *ENPP2*, *PITPNA*); (iii) oxidoreductase activity (e.g. *PCYOX1*, *STCH*, *ALDH1A3*, *CDO1*, *BDH2*, *FADS1*); (iv) pigment biosynthesis and melanin biosynthesis [e.g. *GPR143*, *TYRP1*, dopachrome tautomerase (DCT), *SILV*]; (v) phagocytic activity (*LAMP2*, *VDP*, *GULP1*); (vi) transporter activity (e.g. *SLC39A6*, *SLC4A2*, *SLC16A1*, *SLC16A4*) (Fig. 3C and Table 1).

Based on the rEx levels, the 154 RPE ‘signature genes’ in anRPE, fn RPE, fcRPE and acRPE preparations can be clustered into four groups (Fig. 4 and Supplementary Material, Table S1). Cluster 1 consists of genes that are on average three times more highly expressed in native fetal compared with the native adult RPE. These genes are involved in extracellular matrix (ECM) formation, tissue remodeling, cytoskeleton reorganization and trafficking, and can be used as sentinels for cell culture-induced alterations in gene expression. Cluster 2 identifies genes whose expression levels are high and relatively

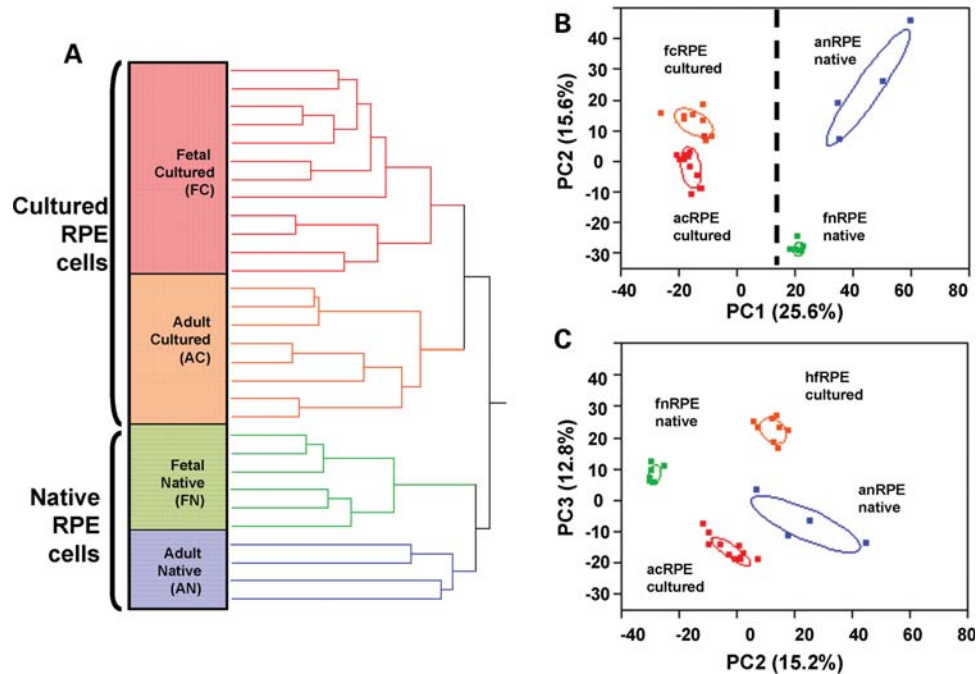


Figure 2. Hierarchical clustering (A), and biplots of the three predominant principal components [PC1, PC2, PC3], (B) and (C) demonstrate that RPE samples separated into two major groups as a result of culture, regardless of the sample origin (adult or fetal). Microarray gene expression analysis of 54 675 probe sets was performed using 30 samples from fetal cultured, fetal native, adult native RPE and ARPE-19 cells. Principal components analysis (which rotates the original 30 data vectors into a new set of 30 vectors whose principal components, or PCs, are uncorrelated and ordered by descending magnitude) was applied to reduce the dimensionality of the data and allow for visualization and clustering. Data also show that all the RPE samples from the same culture or tissue category grouped together, ruling out potential misclassifications. Ellipses indicate 50% confidence levels for each tissue type. Percentage values next to each PC indicate the proportion of total variation in the original 30 by 54 675 data matrix represented by each principal component. Thus, the three predominant components represent the majority ($54\% = 25.6 + 15.6 + 12.8$) of the total variation among the 30 samples on the 54 675 probe sets (85). There is a greater heterogeneity among the adult native RPE gene expression profiles, compared with the other three groups. Expression profiles under controlled culture conditions are expected to be more homogeneous than those from native tissue from different individuals. The four adult native RPE tissues were from individuals with a 25 year age range, while the fetal tissues were from a limited gestational age range (16–18 weeks).

unchanged among the four RPE preparations; these include genes involved in visual cycle, pigment biosynthesis, transporter activity and cell signaling. Cluster 3 is similar to Cluster 2, but with lower levels of gene expression. Cluster 4 includes an important group of 17 genes that exhibit 26–87 times lower expression in ARPE-19 cells when compared with native and fetal cultured RPE. Functional groups (GO terminology) represented in this cluster include (i) transporters; (ii) growth factors and transcriptional regulators; (iii) signaling proteins and (iv) visual cycle components.

Validation of RPE ‘signature’ genes

Expression levels of RPE signature genes were validated by qRT-PCR in preparations from donor RPE ($n \geq 2$) and in a panel of human tissues and cell cultures from native fetal retina, native and cultured fetal choroid, brain, melanocytes, colon, intestine, kidney, liver, lung, trachea, calu-3 cells, a tissue-mix and testes. The correlation coefficient between \log_{10} -transformed qRT-PCR and the \log_{10} -transformed microarray expression levels were calculated for each RPE group. For the microarray data, the rEx value for each gene was calculated relative to the median of the corresponding gene in a validation panel of 11 tissues (Supplementary Material, Table S1). Three tissues (native fetal retina, native

and cultured fetal choroid) were excluded from the validation set because of their physical proximity to RPE and the possibility of contamination by RPE. The mean rEx for each gene by qRT-PCR in fetal-cultured RPE, adult-cultured RPE/ARPE-19, fetal native RPE and adult native RPE samples showed a significant correlation ($P < 0.0001$) with the microarray data in each RPE sample type. The correlation coefficient is 0.74 for cultured fetal RPE, 0.94 for the adult cultured/ARPE-19, 0.83 for fetal native RPE, and 0.76 for native adult tissue.

Hierarchical clustering of tested samples (Fig. 5) demonstrates a distinct segregation of RPE samples (shown above the yellow line) from 14 other tested tissues, as revealed by the expression of 150 signature genes. The qPCR levels of RPE signature genes (Supplementary Material, Table S1) segregate into two major clusters according to the level of variation of their rEx between native and cultured RPE groups and within each RPE group. Cluster 1 includes ‘commonly expressed RPE genes’ that are, for the most part, three to four orders of magnitude more highly expressed in the RPE samples relative to the validation set. The dashed box in Cluster 2 indicates genes that are ≈ 100 -fold more highly expressed in native RPE (fetal and adult) when compared with cultured RPE and with the validation set. In contrast, the expression levels of ‘commonly expressed RPE

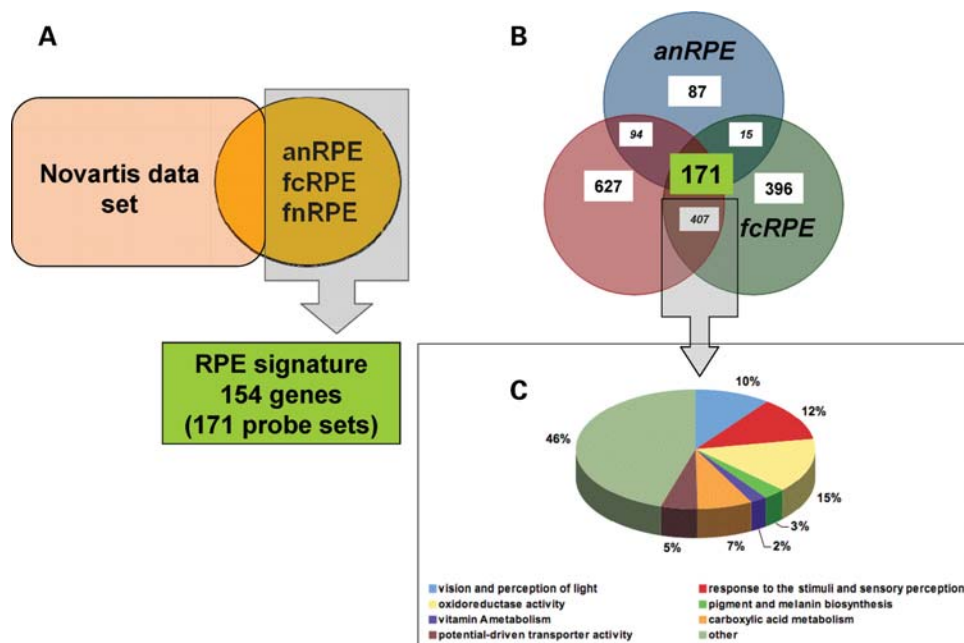


Figure 3. (A) Identification of RPE signature genes common among native fetal, adult native and fetal cultured RPE cells compared with the expression the same genes in the Novartis anatomically diverse data set (A). RPE-specific genes were determined through the selection of genes with relative expression (rEx) values of 10 or greater in each RPE group when their mean expression values were compared with the median gene expression value of all 78 Novartis tissues (SymAtlas, <http://wombat.gnf.org/index.html>). (B) Venn diagram showing the number of genes with $rEx \geq 10$ in AN, FN and FC RPE preparations and the number of common 'signature' genes between these lists when compared with the Novartis panel. (C) GO Biological process functional groups overrepresented in the RPE signature as determined by the EASE analysis (EASE score $P < 0.005$).

genes' are consistently high in almost all RPE preparations (excluding ARPE19; dotted box, Cluster 1) and therefore are not substantially affected either by culturing or by the choice of model (fetal *versus* adult or native *versus* cultured). We suggest that these genes can be used as RPE markers.

Culturing RPE cells can alter the expression of 'signature' genes. To evaluate this further, we calculated the relative decrease in expression for all signature genes in AC (ARPE-19) and FC RPE relative to adult RPE. In both cases, the median decrease is ≈ 3 -fold. The expression of a given gene was considered unchanged if it was similar to native adult RPE expression. However, some genes express at drastically lower levels (up to 1000-fold lower) in ARPE-19, but not in FC RPE (Supplementary Material, Table S1). In ARPE-19, 74 of 150 of the signature genes are expressed at lower levels when compared with adult native RPE. In comparison, only 34 of 150 are expressed at reduced level in FC RPE when compared with adult native RPE.

Differential expression of selected RPE genes was validated by immunoblot analysis. Protein levels of TYRP1, BEST1, CDH3, CRX, CHRNA3, RPE65 were determined in fetal RPE cultures (three donors) and ARPE-19 cell cultures (Fig. 6A). As predicted by qRT-PCR and microarray analysis, protein levels of TYRP1 were similar between the RPE models, whereas the levels of other proteins, including BEST1, CDH3, CRX, CHRNA3, RPE65, were dramatically reduced in ARPE-19 cultures. Immunoblot analyses also demonstrated high expression of RPE65, BEST1, SILV1, CHD3, CHRNA3 and SERP1F1 proteins in RPE when compared with other tissues tested (Fig. 6B).

Cross-sectional analysis of the RPE signature genes against AMD-GWAS

Early changes in AMD include RPE dysfunction (27). To check the potential contribution of RPE-enriched 'signature' genes to AMD, we examined ~ 2.5 million genotyped and imputed single nucleotide polymorphisms (SNPs) in 2157 AMD cases and 1150 controls (28). Among these SNPs, we focused on those with at least 1% minor allele frequency and within 100 kb of the 5' and 3' end of each of the 154 RPE 'signature' genes, resulting in a set of 33 096 SNPs for evaluation. For each of these, we examined the association with AMD in the GWAS data set and compared the observed P -values with their chance expectations (assuming none of the variants are associated with AMD; Fig. 7). The most significant association maps near the *TIMP3* gene (rs5754221, $P = 5 \times 10^{-5}$), and other potentially interesting signals, are observed near *GRAMD3* (rs4836255, $P = 3 \times 10^{-4}$), *PITPNA* (rs17821234, $P = 4 \times 10^{-4}$) and *CHRNA3* (rs11072791, $P = 6 \times 10^{-4}$). We note that genotyping of additional AMD case-control samples (25) indeed validated the association of SNPs near *TIMP3* with AMD ($P = 10^{-11}$).

In addition to these four SNPs near 48 other genes show slight association with AMD at a P -value of < 0.01 (Table 2) and may be the candidates for further examination, given the convergence of gene expression data (reported here) and the genetic association data (from the GWAS). The functional classification of these 48 genes by DAVID (29) revealed 18 genes with a signal sequence at N terminus (Fig. 8). All 18 have a central hydrophobic region (red), N-terminal hydrophilic region (green) and a C-terminal flanking region (blue). Notably,

Table 1. Relative expression (rEx)^a values of RPE signature genes^b (154) with rEx ≥ 10 compared to the Novartis data set determined by microarray analysis

Gene symbol	Gene name	Probe set ID	Fold-change AN (n = 4)	FN (n = 4)	FC (n = 4)	AC (n = 8)	PCR Val
ADAM9	ADAM metallopeptidase domain 9 (meltrin gamma)	202381_at	13.9	26.8	52.4	50.3	
ADCY9	Adenylate cyclase 9	204497_at	21.3	29.7	11.2	17.5	
AHR	Aryl hydrocarbon receptor	202820_at	12.1	13.2	11.1	28.7	•
ALDH1A3	Aldehyde dehydrogenase 1 family, member A3	203180_at	37.2	342.3	51.4	247.5	
ANKRD12	Ankyrin repeat domain 12	216550_x_at	22.8	22.0	10.4	12.8	
APLP1	Amyloid beta (A4) precursor-like protein 1	209462_at	28.7	80.1	38.8	48.4	
ARL6IP1	ADP-ribosylation factor-like 6 interacting protein 1	211935_at	14.1	23.5	12.2	9.3	
ARMC9	Armadillo repeat containing 9	219637_at	12.0	10.1	16.3	13.0	
ASAH1	N-acylsphingosine amidohydrolase (acid ceramidase) 1	210980_s_at	13.9	31.3	13.3	18.2	
ATF1	Activating transcription factor 1	222103_at	10.4	24.3	15.7	23.3	•
BAT2D1	BAT2 domain containing 1	211947_s_at	14.4	13.3	11.1	11.1	
BCLAF1	BCL2-associated transcription factor 1	201101_s_at	16.4	13.7	25.8	15.8	•
BDH2	3-Hydroxybutyrate dehydrogenase, type 2	218285_s_at	13.0	22.6	13.6	16.9	
BEST1	Bestrophin 1	207671_s_at	53.5	167.6	31.4	1.5	
BHLHB3	Basic helix-loop-helix domain containing, class B, 3	221530_s_at	11.9	16.2	11.9	14.6	
BMP4	Bone morphogenetic protein 4	211518_s_at	61.8	158.0	38.4	45.6	
C1orf108	Akirin 1	217893_s_at	10.6	14.6	16.1	14.7	
C20orf19	Chromosome 20 open-reading frame 19	219961_s_at	10.6	21.4	14.7	15.2	
CALU	Calumenin	200755_s_at	11.3	25.2	67.6	53.8	
CDH1	Cadherin 1, type 1, E-cadherin (epithelial)	201131_s_at	13.8	51.7	26.3	8.1	•
CDH3	Cadherin 3, type 1, P-cadherin (placental)	203256_at	10.6	64.6	30.7	3.4	
CDO1	Cysteine dioxygenase, type 1	204154_at	14.4	57.9	10.5	3.0	
CHRNA3	Cholinergic receptor, nicotinic, alpha 3	210221_at	35.0	52.8	39.1	1.2	
CHRNA3	Cholinergic receptor, nicotinic, alpha 3	211772_x_at	28.3	32.2	29.5	0.9	
CLCN4	Chloride channel 4	214769_at	45.6	107.0	21.8	16.4	
COL8A2	Collagen, type VIII, alpha 2	221900_at	12.2	132.0	38.4	21.0	
COX15	COX15 homolog	221550_at	13.6	14.2	18.7	13.6	
CRIM1	Cysteine-rich transmembrane BMP regulator 1	202552_s_at	21.8	27.6	28.5	55.2	
CRIM1	Cysteine-rich transmembrane BMP regulator 1	202551_s_at	11.7	12.3	17.9	35.4	
CRX	Cone-rod homeobox	217510_at	41.9	14.3	11.8	0.2	
CSPG5	Chondroitin sulfate proteoglycan 5 (neuroglycan C)	39966_at	19.2	102.8	22.4	5.0	
CTBP2	C-terminal binding protein 2	201218_at	12.8	29.1	11.0	10.2	
CYP20A1	Cytochrome P450, family 20, subfamily A, polypeptide 1	219565_at	10.2	15.6	18.0	21.2	
DAP3	Death-associated protein 3	208822_s_at	12.4	27.0	29.3	27.9	
DCT	Dopachrome tautomerase	205337_at	12.6	304.6	131.2	12.0	
DCUN1D4	DCN1, defective in cullin neddylation 1	212855_at	10.6	19.4	17.4	24.5	
DEGS1	Degenerative spermatocyte homolog 1	209250_at	10.7	10.8	18.3	22.7	•
DHPS	Deoxyhypusine synthase	207831_x_at	10.8	19.8	15.8	12.7	
DIXDC1	DIX domain containing 1	214724_at	10.9	18.5	13.2	29.8	
DMXL1	Dmx-like 1	203791_at	12.4	50.4	14.5	14.4	
DNAJB14	DnaJ (Hsp40) homolog, subfamily B, member 14	219237_s_at	13.6	14.6	10.2	10.1	
DUSP4	Dual specificity phosphatase 4	204014_at	75.8	268.0	427.5	40.0	
DUSP4	Dual specificity phosphatase 4	204015_s_at	22.8	46.1	103.6	10.7	
DZIP1	DAZ interacting protein 1	204557_s_at	10.7	32.7	26.8	19.0	
EFEMP1	EGF-containing fibulin-like extracellular matrix protein 1	201843_s_at	28.3	51.0	28.0	111.8	
EFEMP1	EGF-containing fibulin-like extracellular matrix protein 1	201842_s_at	22.5	28.8	23.9	52.6	
EFHC1	EF-hand domain (C-terminal) containing 1	219833_s_at	16.0	38.6	41.3	54.1	
EID1	EP300 interacting inhibitor of differentiation 1	211698_at	16.6	26.7	13.7	25.2	
ENPP2	Ectonucleotide pyrophosphatase/phosphodiesterase 2	209392_at	33.2	71.8	12.1	39.0	
FADS1	Fatty acid desaturase 1 /// fatty acid desaturase 3	208963_x_at	15.0	42.0	39.5	27.6	
FAM18B	Family with sequence similarity 18, member B	218446_s_at	14.1	17.9	16.7	18.0	

FGFR2	Fibroblast growth factor receptor 2	203638_s_at	21.3	148.4	45.8	1.0	
FOXD1	Forkhead box D1	206307_s_at	10.8	88.4	30.2	30.0	
FRZB	Frizzled-related protein	203698_s_at	84.3	314.0	183.7	0.4	
FRZB	Frizzled-related protein	203697_at	38.9	115.3	53.6	0.1	
GAS1	Growth arrest-specific 1	204457_s_at	12.5	51.6	19.5	33.4	
GEM	GTP-binding protein overexpressed in skeletal muscle	204472_at	23.3	53.1	16.7	52.3	
GJA1	Gap junction protein, alpha 1, 43 kDa	201667_at	11.6	50.7	31.7	38.6	
GOLPH3L	Golgi phosphoprotein 3-like	218361_at	13.4	17.3	15.2	18.7	•
GPM6B	Glycoprotein M6B	209170_s_at	25.1	62.4	11.3	0.2	
GPNMB	Glycoprotein (transmembrane) nmb	201141_at	17.5	32.3	64.1	70.0	
GPR143	G protein-coupled receptor 143	206696_at	12.6	153.8	64.8	53.6	
GRAMD3	GRAM domain containing 3	218706_s_at	15.1	18.1	15.4	17.5	
GULP1	GULP, engulfment adaptor PTB domain containing 1	215913_s_at	18.4	103.4	84.2	25.3	
GULP1	GULP, engulfment adaptor PTB domain containing 1	204235_s_at	15.4	81.9	35.6	14.2	
GULP1	GULP, engulfment adaptor PTB domain containing 1	204237_at	19.8	82.7	38.8	19.0	
HSP90B1	Heat shock protein 90 kDa beta (Grp94), member 1	216449_x_at	15.5	34.7	110.9	61.1	
IFT74	Intraflagellar transport 74 homolog (<i>Chlamydomonas</i>)	219174_at	36.7	73.5	44.2	73.5	
IGF2BP2	Insulin-like growth factor 2 mRNA-binding protein 2	218847_at	10.4	38.0	20.3	18.3	
ITGAV	Integrin, alpha V	202351_at	31.4	53.1	29.5	47.5	
ITM2B	Integral membrane protein 2B	217731_s_at	18.6	21.8	13.5	27.6	N
KLHL21	Kelch-like 21 (<i>Drosophila</i>)	203068_at	14.8	25.8	23.6	24.9	
KLHL24	Kelch-like 24 (<i>Drosophila</i>)	221986_s_at	12.9	22.5	23.7	15.0	
LAMP2	Lysosomal-associated membrane protein 2	200821_at	10.6	20.9	12.6	19.5	
LAPTM4B	Lysosomal protein transmembrane 4 beta	208029_s_at	12.0	20.9	18.5	13.8	
LAPTM4B	Lysosomal protein transmembrane 4 beta	214039_s_at	13.6	18.3	14.8	12.0	
LGALS8	Lectin, galactoside-binding, soluble, 8	208933_s_at	15.7	23.3	16.2	31.8	•
LHX2	LIM homeobox 2	206140_at	36.7	335.8	348.6	161.1	
LIMCH1	LIM and calponin homology domains 1	212328_at	10.1	29.6	14.5	50.1	
LIN7C	Lin-7 homolog C (<i>C. elegans</i>)	221568_s_at	22.6	37.3	18.1	27.7	
LOXL1	Lysyl oxidase-like 1	203570_at	21.7	233.9	195.5	243.1	
LSR	Lipolysis-stimulated lipoprotein receptor	208190_s_at	16.7	15.3	11.6	10.9	
MAB21L1	mab-21-like 1 (<i>C. elegans</i>)	206163_at	20.6	70.5	41.9	87.3	
MANEA	Mannosidase, endo-alpha	219003_s_at	14.7	30.8	21.6	27.5	
MAP9	Microtubule-associated protein 9	220145_at	39.6	103.1	57.2	40.5	
MBNL2	Muscleblind-like 2 (<i>Drosophila</i>)	203640_at	10.9	10.4	13.9	16.3	•
MED8	Mediator complex subunit 8	213126_at	19.5	39.9	23.0	25.7	
MET	Met proto-oncogene (hepatocyte growth factor receptor)	203510_at	64.0	224.2	78.0	191.5	
MFAP3L	Microfibrillar-associated protein 3-like	205442_at	49.1	60.3	46.1	56.2	
MPDZ	Multiple PDZ domain protein	213306_at	10.5	22.4	12.1	16.5	
MPHOSPH9	M-phase phosphoprotein 9	215731_s_at	14.3	31.9	12.3	15.0	
MPHOSPH9	M-phase phosphoprotein 9	206205_at	14.2	23.7	19.5	15.0	
MYRIP	Myosin VIIA and Rab interacting protein	214156_at	97.7	95.6	51.2	47.0	
NAV3	Neuron navigator 3	204823_at	13.3	128.0	22.9	27.7	
NDC80	NDC80 homolog, kinetochore complex component	204162_at	11.8	20.3	11.2	6.7	
NEDD4L	Neural precursor cell expressed	212448_at	11.5	23.3	17.4	9.1	
NOL8	Nucleolar protein 8	218244_at	14.1	39.4	33.7	32.6	N
NRIP1	Nuclear receptor interacting protein 1	202600_s_at	32.5	50.2	22.1	38.2	
NUDT4	Nudix (nucleoside diphosphate-linked moiety X)	212183_at	11.0	11.0	13.5	29.6	•
OSTM1	Osteopetrosis-associated transmembrane protein 1	218196_at	10.1	13.5	12.4	11.5	
PAK1IP1	PAK1 interacting protein 1	218886_at	14.1	31.2	17.8	31.0	
PCYOX1	Prenylcysteine oxidase 1	203803_at	16.6	16.4	22.8	23.6	
PDPN	Podoplanin	221898_at	14.8	81.2	30.7	26.7	
PDZD8	—	213549_at	10.6	29.6	15.1	11.8	
PHACTR2	Phosphatase and actin regulator 2	204049_s_at	14.5	40.0	10.6	24.8	
PITPNA	Phosphatidylinositol transfer protein, alpha	201191_at	29.2	63.3	11.3	9.2	

Continued

Table 1. Continued

Gene symbol	Gene name	Probe set ID	Fold-change AN (n = 4)	FN (n = 4)	FC (n = 4)	AC (n = 8)	PCR Val
PKNOX2	PBX/knotted 1 homeobox 2	222171_s_at	11.9	47.0	13.9	1.5	
PLAG1	Pleiomorphic adenoma gene 1	205372_at	10.2	43.9	14.6	3.0	
PLCB4	Phospholipase C, beta 4	203896_s_at	11.8	30.1	27.2	95.7	
PLOD2	Procollagen-lysine, 2-oxoglutarate 5-dioxygenase 2	202620_s_at	13.4	11.1	82.3	82.4	
PRNP	Prion protein	201300_s_at	12.1	18.0	10.3	14.6	
PSME4	Proteasome (prosome, macropain) activator subunit 4	212219_at	13.1	15.2	20.4	19.1	
PTGDS	Prostaglandin D2 synthase 21 kDa (brain)	211663_x_at	11.2	14.9	10.6	1.2	
PTPRG	Protein tyrosine phosphatase, receptor type, G	204944_at	15.8	55.4	13.4	7.3	
RAB38	RAB38, member RAS oncogene family	219412_at	14.1	75.5	15.1	19.3	
RBM34	RNA-binding motif protein 34	214943_s_at	11.4	15.2	34.4	18.3	•
RBP1	Retinol-binding protein 1, cellular	203423_at	31.7	61.3	15.5	6.5	
RDH11	Retinol dehydrogenase 11 (all-trans/9-cis/11-cis)	217776_at	24.4	17.4	18.0	12.4	
RHOBTB3	Rho-related BTB domain containing 3	202976_s_at	11.5	17.3	11.7	9.0	
RNF13	Ring finger protein 13	201780_s_at	12.3	18.6	11.2	26.9	
RPE65	Retinal pigment epithelium-specific protein 65 kDa	207107_at	277.1	375.7	13.3	8.5	
RRAGD	Ras-related GTP binding D	221524_s_at	34.8	65.8	30.0	37.4	
SAS10	UTP3, small subunit (SSU) processome component	209486_at	12.1	22.3	25.2	26.5	N
SCAMP1	Secretory carrier membrane protein 1	212417_at	20.7	35.3	15.5	21.6	
SDC2	Syndecan 2	212158_at	18.3	53.8	36.0	31.8	
SEMA3C	Sema domain, short basic domain, (semaphorin) 3C	203789_s_at	11.8	50.7	46.5	66.8	
SERPINF1	Serpin peptidase inhibitor,	202283_at	36.1	51.0	36.2	20.5	
SFRP5	Secreted frizzled-related protein 5	207468_s_at	40.8	233.6	23.3	2.0	
SGK3	Chromosome 8 open-reading frame 44 /	220038_at	43.5	159.3	26.9	49.6	
SIL1	SIL1 homolog, endoplasmic reticulum chaperone	218436_at	10.4	14.2	20.5	28.0	
SILV	Silver homolog (mouse)	209848_s_at	14.5	104.5	71.8	8.9	
SIX3	SIX homeobox 3	206634_at	10.5	36.1	11.6	13.7	
SLC16A1	Solute carrier family 16, member 1	202235_at	27.6	64.5	46.5	41.1	
SLC16A1	Solute carrier family 16, member 1	202234_s_at	13.4	25.8	17.8	19.2	
SLC16A1	Solute carrier family 16, member 1	209900_s_at	60.1	113.2	95.3	78.1	
SLC16A4	Solute carrier family 16, member 1	205234_at	71.1	83.6	12.8	93.5	
SLC24A1	Solute carrier family 24	206081_at	50.6	16.1	15.2	13.2	
SLC39A6	Solute carrier family 39 (zinc transporter), member 6	202088_at	13.6	24.4	16.8	17.4	
SLC4A2	Solute carrier family 4, anion exchanger	202111_at	20.9	104.6	35.8	64.8	
SLC6A15	Solute carrier family 6 (neutral amino acid transporter)	206376_at	21.4	128.7	171.9	12.8	
SLC6A20	Solute carrier family 6 (proline IMINO transporter)	219614_s_at	35.2	156.9	21.8	5.3	
SMAD6	SMAD family member 6	207069_s_at	13.3	37.2	27.8	41.3	
SMC3	Structural maintenance of chromosomes 3	209258_s_at	13.9	23.7	14.7	13.5	
SORBS2	Sorbin and SH3 domain containing 2	204288_s_at	22.5	79.6	15.5	22.1	
SOSTDC1	Sclerostin domain containing 1	213456_at	54.7	598.7	46.2	0.3	
SPAST	Spastin	209748_at	10.1	22.8	11.8	13.6	
STAM2	Signal transducing adaptor molecule	209649_at	32.0	41.4	45.5	49.7	
STCH	Heat shock protein 70 kDa family, member 13	202557_at	11.0	14.9	18.1	11.9	
SULF1	Sulfatase 1	212354_at	16.1	84.4	14.4	9.0	
SULF1	Sulfatase 1	212353_at	20.9	107.6	14.3	8.9	
TAX1BP1	Tax1	213786_at	12.9	28.7	12.3	15.0	
TFPI2	Tissue factor pathway inhibitor 2	209278_s_at	155.9	169.2	31.2	894.7	
TIMP3	TIMP metalloproteinase inhibitor 3	201147_s_at	14.9	22.8	28.8	58.1	
TIMP3	TIMP metalloproteinase inhibitor 3	201150_s_at	25.6	31.1	20.7	35.6	
TRPM1	Transient receptor potential cation channel	206479_at	32.2	229.0	43.0	23.0	
TTL4	Tubulin tyrosine ligase-like family, member 4	203702_s_at	14.5	157.0	42.9	6.1	
TTR	Transthyretin	209660_at	178.8	155.1	49.2	1.8	
TYRP1	Tyrosinase-related protein 1	205694_at	234.8	307.3	222.9	191.8	

UBL3	Ubiquitin-like 3	201534_s_at	12.1	12.8	15.2	21.4	
USP34	Ubiquitin-specific peptidase 34	212065_s_at	21.1	37.3	61.0	48.4	
VDP	USO1 homolog, vesicle docking protein (yeast)	201831_s_at	12.0	14.3	24.7	14.8	N
VEGFA	Vascular endothelial growth factor A	210512_s_at	15.8	55.5	54.1	45.2	•
WASL	Wiskott-Aldrich syndrome-like	205809_s_at	14.7	12.5	13.1	16.4	
WWC2	WW and C2 domain containing 2	218775_s_at	12.3	38.6	31.9	41.6	
WWTR1	WW domain containing transcription regulator 1	202133_at	10.8	56.8	20.5	32.6	N
ZNF19, -23	Zinc finger protein 23 (KCOX 16)	213934_s_at	12.2	23.6	23.7	23.5	N
40064	Septin 8	209000_s_at	10.6	15.7	15.8	16.7	N
—	—	222294_s_at	12.0	33.0	19.8	12.9	N
—	—	AFFX-r2-Bs-dap-3_at	323.6	115.9	173.7	161.2	N
—	—	AFFX-DapX-3_at	142.6	46.6	80.9	74.9	N
—	—	AFFX-r2-Bs-dap-M_at	62.3	12.1	32.9	32.1	N

^aEx values were calculated as the ratio of mean of gene expression values in four RPE sample types (AN, FN, FC and AC) over the median expression value across 78 diverse anatomical samples (Genomics Institute of Novartis Research Foundation tissue data set). The black dots indicate genes that were not corroborated by qRT-PCR and the letter N indicates genes for which qRT-PCR data are not available. ^bA gene was defined to be an RPE-signature gene if its rEx was ≥ 10 for ALL three RPE preparations (native adult and fetal RPE and primary culture of fetal RPE).

coding regions of these genes include many variants that potentially could contribute to protein misfolding.

In a separate analysis, we utilized a catalog of SNPs [called expression quantitative trait loci (eQTLs)] known to be associated with expression levels of specific genes (30). From this catalogue, we selected a list of 44 SNPs (Supplementary Material, Table S2) associated with expression levels of some of the genes in the RPE signature set ($P < 10^{-7}$). Four of these SNPs exhibited nominal association with AMD at $P < 0.05$ (compared with two expected by chance); these eQTLs are rs12150474 (associated with expression of *PHACTR2* at $P < 10^{-7}$ and with AMD with $P = 0.007$); rs7105701 (*RAB38* with $P < 10^{-7}$; AMD with $P = 0.01$); rs1483539 (*LGALS8* with $P < 10^{-8}$; AMD with $P = 0.03$) and rs2449517 (*LAPTM4B* with $P < 10^{-8}$; AMD with $P = 0.04$).

Role of DCT in RPE physiology

Epithelia are characterized by the asymmetric distribution of plasma membrane proteins. This polarity fundamentally contributes to a range of functions that allow the epithelium to support the health and integrity of surrounding cells. The present data show that DCT is highly expressed in human RPE (Table 1; Supplementary Material, Fig. S1). Previous studies have indicated a role for this gene product in pigment development and the modulation of cell responses to oxidative stress (31,32). In Figure 9A, we used a lentivirus system to deliver specific shRNA to reduce DCT levels (clone 38) by $\approx 75\%$ in hRPE. A similar reduction was observed in two additional experiments. This treatment caused a significant reduction in the transepithelial resistance (TER) of confluent monolayers from 842 ± 222 to $328 \pm 171 \Omega \text{ cm}^2$ ($n = 6$; $P < 0.05$). A comparison of Fig. 9C and F show that transduction of hRPE cells with DCT38 clone shRNA a dramatically reduced intracellular DCT levels (Fig. 9F). Reduction of DCT levels also led to a significant reorganization of fully polarized RPE cytoskeleton. For example, a comparison of Figure 9D and G show that the apical localization of ezrin is totally disrupted with an apparent loss of its normal apical membrane polarity. Finally, Figure 9E and H show RPE F-actin fibers are disrupted to a more diffuse pattern throughout the cells. These data indicate that DCT, a highly expressed human RPE signature gene, is critical for the maintenance of normal epithelial phenotype.

DISCUSSION

The RPE is fundamentally important for retinal development and function, and is a critical focus of retinal degenerative diseases and therapeutic intervention. Although RPE is functionally distinct from other epithelial cells and its pathophysiology is under intense investigation, relatively little is known about the set of genes that distinguish the RPE phenotype. The gene expression profile of a cell should reflect its morphological and functional specificity as well as molecular and physiological signaling pathways. The present study provides, for the first time, a specific gene expression signature of normal human RPE. We generated global expression profiles of human RPE (native and cultured cells) and identified 154

Signature gene expression levels (microarray)

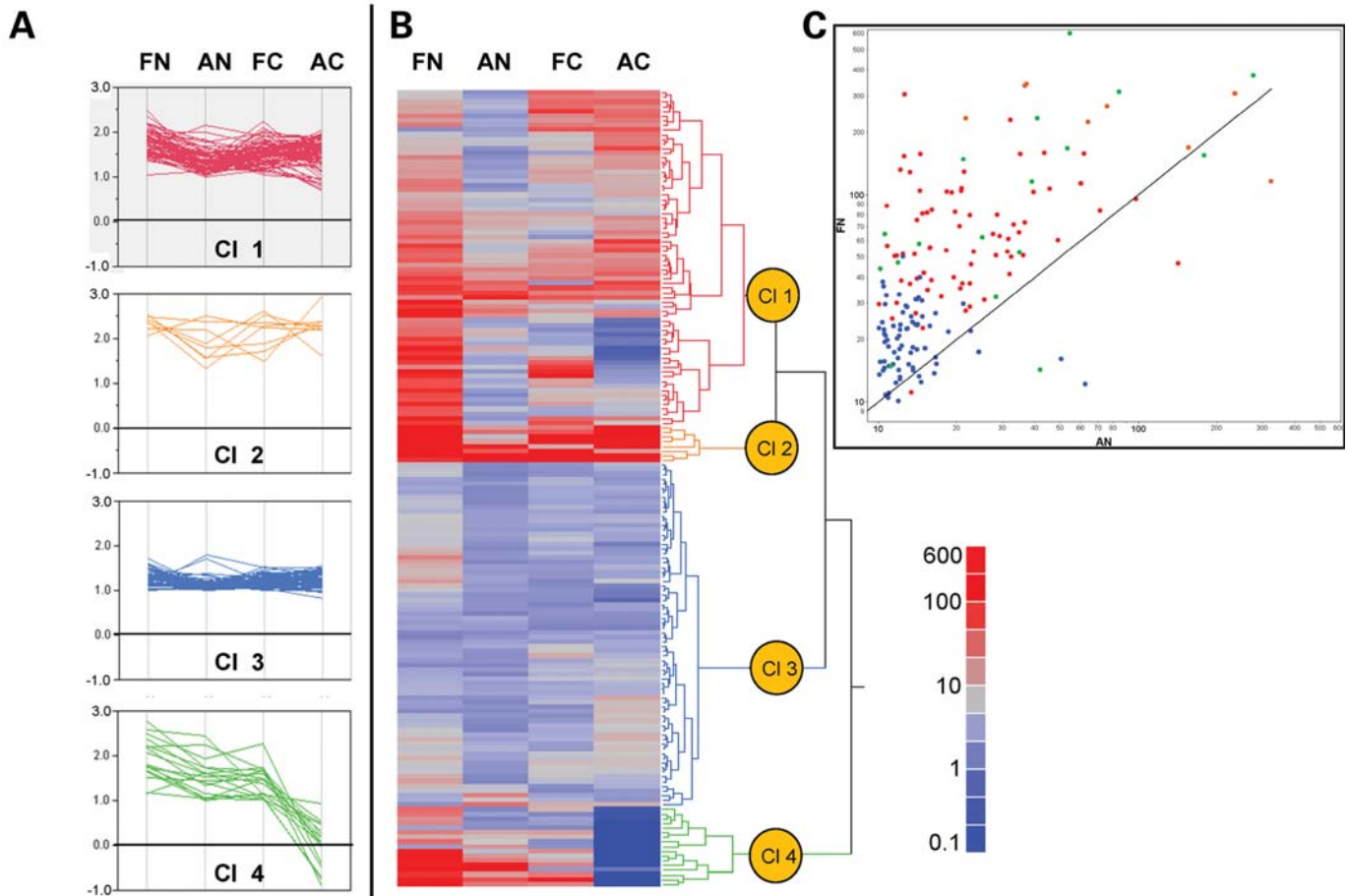


Figure 4. Cluster analysis performed on the profiles of 154 RPE-specific genes (171 probe sets) determined from microarray analysis on adult native RPE (AN) tissues, native fetal tissues (FN), fetal cultured RPE (FC) and ARPE-19 (AC). (A) Gene clusters (CI 1–CI 4) reflect different relative expression (rEx) patterns of the RPE-specific genes for each of the four RPE preparations. (B) Each horizontal colored band represents mean rEx of a single gene in each RPE preparation with the color-bar, showing the numerical rEx value. The cluster dendrogram on the right-hand side of the heat map groups the genes into the clusters represented in (A). (C) Log–log plot of signature gene-rEx of fetal native (FN - vertical axis 0–600 of rEx values) and adult native (AN - horizontal axis 0–600 of rEx values) RPE. Genes above the unity line have a higher expression level in fetal native compared with adult native RPE.

genes that exhibit 10-fold or higher expression when compared with the median of Novartis data set of various transcriptomes. Somewhat lesser stringent criteria of 5-fold or higher expression increased the list of RPE genes to 919 probe sets. We suggest that the 154 highly expressed genes, reported here, can serve as a ‘unique’ functional signature of RPE and can discriminate it from other epithelia or cell types.

Because of RPE’s relevance to retinal disease, the RPE ‘signature’ gene set is of value for identifying candidate genes for genetic analysis or physiological studies. Ingenuity pathway analysis, together with the RetNet database (www.sph.uth.tmc.edu/retnet/home.htm), revealed 17 RPE signature genes that are involved in ocular disorders (*TYRP1*, *SIL1*, *BEST1*, *COL8A2*, *EFEMP1*, *LOXLI*, *SERPINF1*, *BMP4*, *VEGFA*, *TIMP3*, *CHRNA3*, *PRNP*, *RPE65*, *CRX*, *GPNMB*, *CDH1*, *CDH3*). In addition, our analysis of RPE signature genes identified a number of newly discovered disease-associated genes. For example, GRP143 was not included by ingenuity in the list of disease-associated genes, but mutations in this gene were

reported to cause X-linked ocular albinism (*OAI*) (33–35). Another example is a discovery of two SNPs in the *LOXLI* gene, recently associated with strong genetic risk for pseudoexfoliation (PEX) syndrome and PEX glaucoma and involved in the formation of choroidal neovascularization (36,37). Using the RetNet database (<http://www.sph.uth.tmc.edu/retnet/>), we also identified 25 of the RPE signature genes within the critical genomic region for retinal degenerative disease loci (Table 3). The disease-causing genes within these loci have not been identified, but the signature genes should be considered as possible candidates, given the critical functional interactions between the RPE and the neural retina. For example, neuroglycan C plays an important role in retinal development and is found to be up-regulated in a mouse model of retinal degeneration (38). In addition, *PITPRG* might be a candidate for AMD (GWAS $P = 0.00065$; Table 2). Another interesting example is the disease-associated locus *MCDR3* (macular dystrophy, retinal 3) that includes RPE signature genes *SCAMP1* and *RHOBTB3*. These two genes play a major role in regulating cell traffic,

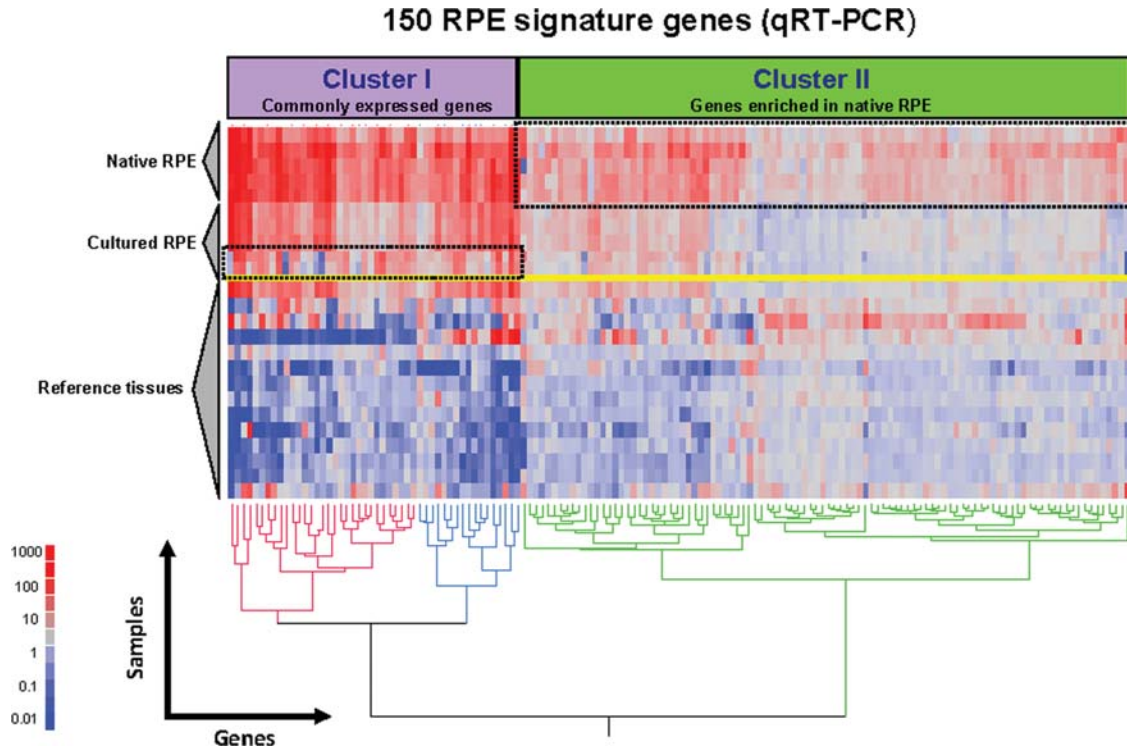


Figure 5. Cluster dendrogram obtained from hierarchical clustering of RPE signature genes determined by qRT-PCR. The dendrogram represents signature gene transcript levels (ΔC_t compared with five housekeeping genes) for four RPE preparations (AN, $n = 2$; FN, $n = 3$; FC, $n = 3$; and AC/ARPE-19, $n = 2$), and a validation set of 14 other tissues and cultures demarcated by the horizontal dotted line. Starting at the bottom of the figure, the validation tissues are: the brain, colon, intestine, kidney, liver, lung testes, trachea, calu3, tissue mix, melanocyte, human fetal retina, human fetal choroid and cultured human choroid RPE. The later three tissues are adjacent to RPE and may therefore contain RPE contamination and are therefore not included in the fold-change calculations. RPE signature genes are plotted horizontally and the tissues are plotted vertically. Each vertical colored band corresponds to expression values for one of the 150 genes in different tissue preparations, relative to the mean value for that gene. Cluster analysis clearly separates native RPE, cultured RPE and 'other tissues.' Cluster I contains a common set of genes, most of which are three to four orders of magnitude more highly expressed in RPE tissue compared with their counterparts in the validation set. Cluster II highlights (dotted box) genes that are ≈ 100 -fold more highly expressed in native RPE with culture RPE.

endocytosis and exocytosis (39,40), and mutations in these genes could disrupt the polarity of RPE and function leading to retinal (photoreceptor) degeneration.

A surprisingly large number of genes (currently 32) in the RPE signature set have been implicated as potential markers for different types of cancers, and therefore may be critical for the regulation of important RPE functions, including proliferation, migration or signaling. For example, prostaglandin D2 synthase (PTGDS) is a key enzyme in arachidonic acid metabolism and is repressed in premalignant stages of oral epithelial cancers (41). This enzyme is a melanocyte marker that is also elevated in retinal detachments and associated with open-angle glaucoma (42). Syndecan-2 is associated with AMD (Table 2) and found to be over expressed in hepatocellular carcinomas, colon carcinomas, and is involved in the suppression of lung carcinoma metastasis (43,44). Podoplanin (*PDPN*) is a novel marker for human well-differentiated keratinizing squamous cell carcinomas of the epithelium (45,46) and dendritic sarcomas (47). It is also a candidate disease gene for Leber congenital amaurosis (Table 3). Mutations in *ADAM9* (Table 2) have been implicated in the pathogenesis retina/RPE attachment in cone-rod dystrophies (48). In addition, frizzle-related protein 5 (*SFRP5*) is a known inhibitor of the WNT pathway and plays a crucial role in

the development of human cancers and is a candidate gene for X-linked retinal dystrophies (49,50).

Cluster analysis is an important tool for distinguishing the genetic architecture of RPE models. For example, Fig. 4 (Clusters 2 and 3) summarizes a set of genes that are expressed at approximately the same level across all native and cultured tissues. These genes, although expressed at two different levels, are all highly expressed when compared with the Novartis transcriptome and invariant with developmental stage or culture conditions. Therefore, we suggest that they represent a kernel of genes minimally required for RPE phenotype. In addition, we found a group of RPE genes ($n = 26$) that are significantly under expressed in ARPE-19 cultured cells when compared with native tissue and primary culture (Fig. 4A, Cluster 4). Previously, it has been shown that these transformed cell lines lack functional characteristics of native RPE. For example, they have relatively low TER, no visible pigmentation and practically no apical microvilli (51,52). The genes showing low ARPE19 expression can be grouped into the following functional categories: (i) transporter activity; (ii) growth factors and transcriptional regulators; (iii) ECM formation and tissue remodeling; (iv) retinoic and fatty acids metabolism and (v) formation of tight junctions, trafficking and melanogenesis. Not surprisingly, the lack of expression

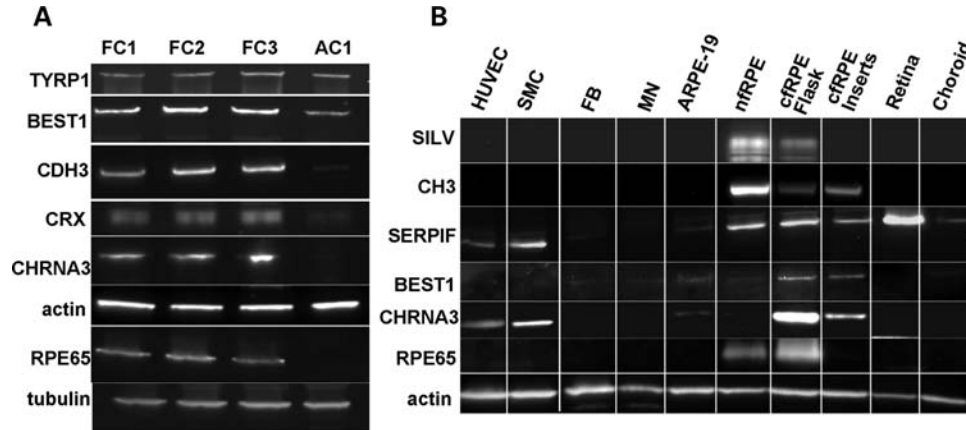


Figure 6. (A) Proteins levels of TYRP1, BEST1, CDH3, CRX, CHRNA3, RPE65 in fcRPE (FC1–FC3, $n = 3$) and ARPE-19 (AC1) cells. Similar to the qRT-PCR data, the TYRP1 levels were not different between the RPE models. The levels of BEST1, CDH3, CHRNA3, RPE65 proteins were dramatically down-regulated in ARPE-19 cultures. (B) The levels of RPE65, BEST1, SILV1, CHD3, CHRNA3, SERPIF1 proteins in fetal native and cultured RPE, ARPE-19, choroids, retina, endothelial cells (HUVEC), smooth muscle cells (SMC), fibroblasts (FB) and circulating monocytes (MN).

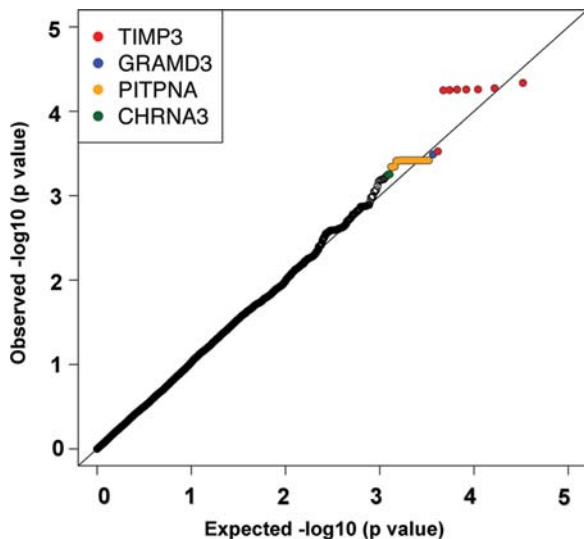


Figure 7. Quantile–quantile (Q–Q) plot of predicted versus observed P -value of SNP's distribution between the AMD and control groups within the region of each gene with 100 kb extension on either side of the 5' and 3' ends of each gene. The figure was generated based on the 33 096 SNPs from GWAS study. Each point on the plot represents an SNP. X -axis is the ordered expected P -values using a $-\log_{10}$ scale, and the y -axis is the observed P -value using a similar scale. Statistical package R 2.8.0 (<http://www.r-project.org/>) was used to generate the plots.

of these proteins can significantly alter normal function of RPE cells (53–57). For example, mice with deletion of *ALDH1A3* (Cluster 5), a key factor regulating synthesis of retinoic acid, die just after birth due to altered epithelial–mesenchymal development (58). A reduced level of *COL8A2* could affect formation of ECM by RPE, which in turn deregulates ability of the cell to proliferate and differentiate (53). Lack of *GPR143* affects melanosomal biogenesis and trafficking leading to the X-linked ocular albinism (OA1) in humans (33,35,59). Reduced expression of these genes in ARPE-19 is probably due to a combination of factors including contami-

nation of the primary cultures by fibroblasts, an excessive number of passages and further de-differentiation compared with primary cultures of fetal human RPE.

Many of the genes in the signature set are differentially expressed between native fetal and adult RPE (Fig. 4A, Cluster 1). This expression difference, confirmed by PCR, is particularly high for the following genes located well above the unity line in Figure 4C: *DCT*, *GPR143*, *SOSTDC1*, *COL8A2*, *FOXD1*, *SILV* and *FGFR2*. Mutations in *COL8A2* gene are linked to Fuchs' endothelial dystrophy and posterior polymorphous dystrophy (60). Mutations in *FGFR2* gene are associated with a variety of CNS disorders such as Crouzon syndrome, Pfeiffer syndrome and Craniosynostosis. Several of these genes may be developmentally important and related to pigment synthesis. Mutations of *GPR143* can affect pigment production in the eye and cause optic changes associated with albinism (35,59) (vide supra). The *DCT* gene product is another example of an enzyme involved in melanin biosynthesis that contributes to RPE homeostasis by detoxifying DOPA-derived metabolites (61). Modulation of *DCT* levels by siRNA substantially affects proliferation in cortical neural progenitor cells (62) and is involved in multidrug resistance (63,64).

The present experiments (Fig. 9) indicate a novel function for *DCT* in maintaining epithelial polarity and tight junction integrity. The shRNA-induced decrease in *DCT* protein expression significantly decreased the total tissue resistance, which in RPE is mainly determined by the resistance of the paracellular (tight junction) pathway (65). Dissolution of epithelial junctions is associated with proliferation and migration and is a precursor of epithelial to mesenchymal transitions, a hallmark of the progression to cancer (65). The reorganization of the cytoskeleton and the loss of polarity following the decrease in *DCT* levels further support this notion. This RPE signature gene joins several recently identified microRNAs enriched in RPE (65) that help maintain a quiescent and polarized state throughout the life of the organism.

Recent linkage and association studies have revealed a number of single nucleotide or other genetic variants that

Table 2. Forty-eight genes from the RPE signature list located in the regions (loci) carrying SNP's significantly associated with AMD ($P < 0.01$) as determined by GWAS

SNP	P-value	Chromosome	Position	RPE gene	Gene in the region
rs5754221	4.60E - 05	22	31433455	<i>TIMP3</i>	<i>SYN3, TIMP3</i>
rs4836255	0.0003231	5	125765866	<i>GRAMD3</i>	<i>RNUXA, ALDH7A1, GRAMD3</i>
rs17821234	0.0003802	17	1383000	<i>PITPNA</i>	<i>TBC1D3B, CCL3L1, CCL4L2, PRPF8, MYO1C, MGC14376, CCL3L3, PITPNA, YWHAE, SKIP, CCL4L1, CRK, SLC43A2, SCARF1, WDR81, RILP</i>
rs11072791	0.0005563	15	76784131	<i>CHRNA3</i>	<i>LOC123688, ADAMTS7, CHRNA3, CHRN4, MORF4L1, CHRNA5, PSMA4</i>
rs1451610	0.0005822	11	87623241	<i>RAB38</i>	<i>RAB38, CTSC</i>
rs2043083	0.0006062	3	150638008	<i>WWTR1</i>	<i>TM4SF1, TM4SF4, WWTR1, TM4SF18</i>
rs4688645	0.0006565	3	61595936	<i>PTRPG</i>	<i>PTRPG</i>
rs17078339	0.0008899	3	45797441	<i>SLC6A20</i>	<i>SLC6A20, FYCO1, LZTFL1, CXCR6, CCR9, SACMIL, LIMD1</i>
rs2083845	0.001021	18	9277340	<i>ANKRD12</i>	<i>ANKRD12, NDUFV2, TWSG1, RALBP1</i>
rs2207189	0.001445	1	169655540	<i>BAT2D1</i>	<i>FMO1, BAT2D1, FMO4</i>
rs17102387	0.001514	10	123406568	<i>FGFR2</i>	<i>ATE1, FGFR2</i>
rs10033615	0.001775	4	171137594	<i>MFAP3L</i>	<i>AADAT, MFAP3L</i>
rs1463729	0.001846	9	125921269	<i>LHX2</i>	<i>NEK6, LHX2, DENND1A</i>
rs10901850	0.001952	10	126697871	<i>CTBP2</i>	<i>ZRANB1, CTBP2, KIAA0157</i>
rs1883931	0.002225	6	52547818	<i>EFHC1</i>	<i>TRAM2, EFHC1, GSTA2, PAQR8, TMEM14A</i>
rs1479024	0.00234	12	76843663	<i>NAV3</i>	<i>NAV3</i>
rs11130146	0.002518	3	47682816	<i>CSPG5</i>	<i>CSPG5, DHX30, SCAP, TMEM103, SMARCC1, MAP4</i>
rs4935917	0.002532	11	124672022	<i>PKNOX2</i>	<i>FEZ1, PKNOX2, LOC219854</i>
rs12375908	0.002636	9	88816922	<i>GAS1</i>	<i>GAS1, FLJ45537</i>
rs1547162	0.002719	13	29382862	<i>UBL3</i>	<i>UBL3, LOC440131</i>
rs10853283	0.003112	18	2705727	<i>NDC80</i>	<i>EMILIN2, METTL4, NDC80, SMCHD1</i>
rs7243360	0.003142	18	54105771	<i>NEDD4L</i>	<i>ALPK2, NEDD4L</i>
rs347240	0.003296	5	72821340	<i>FOXD1</i>	<i>FOXD1, UTP15, BTF3, ANKRA2, RGNEF</i>
rs6828613	0.003311	4	40994249	<i>LIMCH1</i>	<i>UCHL1, LIMCH1, APBB2</i>
rs6750502	0.00362	2	231991153	<i>ARMC9</i>	<i>ARMC9, B3GNT7, C2orf57, C2orf52, NMURI, NCL</i>
rs13173742	0.004548	5	95166326	<i>RHOBTB3</i>	<i>SPATA9, GPR150, RHOBTB3, ARSK, RFESD, ELL2, GLRX</i>
rs10039749	0.004586	5	115256241	<i>CDO1</i>	<i>ATG12, COMMD10, CDO1, FLJ90650, AP3S1</i>
rs12657132	0.0046	5	118600296	<i>DMXL1</i>	<i>TNFAIP8, DMXL1</i>
rs9525029	0.004804	13	95045828	<i>DZIP1</i>	<i>DZIP1, DNAJC3, CLDN10</i>
rs9513227	0.004809	13	96737303	<i>MBNL2</i>	<i>RAP2A, MBNL2</i>
rs1648390	0.005065	11	111225282	<i>DIXDC1</i>	<i>C11orf52, PPP2R1B, DLAT, ALG9, C11orf1, CRYAB, SNF1LK2, LOC91893, HSPB2, DIXDC1</i>
rs2528467	0.005095	7	16486114	<i>SOSTDC1</i>	<i>ANKMY2, LOC442511, SOSTDC1, BZW2, LOC729920</i>
rs11638121	0.00512	15	29212294	<i>TRPM1</i>	<i>TRPM1, MTMR15, KLF13, MTMR10</i>
rs2739733	0.005429	8	18047160	<i>ASAH1</i>	<i>PCMI, ASAH1, NAT1</i>
rs936534	0.005785	2	70428397	<i>PCYOX1</i>	<i>FAM136A, C2orf42, PCYOX1, SNRPG, TIA1, TGFA</i>
rs13144644	0.005873	4	186900916	<i>SORBS2</i>	<i>SORBS2</i>
rs9460922	0.005964	6	10709652	<i>PAK1IP1</i>	<i>MAK, C6orf218, TFAP2A, GCNT2, TMEM14B, PAK1IP1, TMEM14C</i>
rs10113275	0.007136	8	38880340	<i>ADAM9</i>	<i>TACC1, TM2D2, HTRA4, PLEKHA2, ADAM9</i>
rs17029542	0.0077	4	100968373	<i>DNAJB14</i>	<i>DNAJB14, MAP2K1IP1, DAPP1, H2AFZ</i>
rs11189328	0.007749	10	99437994	<i>SFRP5</i>	<i>C10orf132, ANKRD2, CRTAC1, C10orf65, C10orf83, ZFYVE27, UBDT1, MMS19, SFRP5, C10orf62, AVP11, PI4K2A</i>
rs9662167	0.007964	1	13824323	<i>PDPN</i>	<i>PDPN, PRDM2</i>
rs1452312	0.008027	2	183373406	<i>FRZB</i>	<i>NCKAP1, DNAJC10, FRZB</i>
rs9806753	0.008028	15	46953709	<i>EID1</i>	<i>EID1, CEP152, KIAA0256, SHC4</i>
rs11905700	0.008705	20	9220914	<i>PLCB4</i>	<i>PLCB4</i>
rs12051963	0.008999	18	31929324	<i>SLC39A6</i>	<i>SLC39A6, ELP2, C18orf21, P15RS, MOCOS</i>
rs7764938	0.00914	6	144262097	<i>PHACTR2</i>	<i>PHACTR2, LTV1, SF3B5, PLAGL1</i>
rs9824873	0.009229	3	184784468	<i>KLHL24</i>	<i>KLHL6, KLHL24, MCF2L2, YEATS2</i>
rs13131773	0.00958	4	184182880	<i>WWC2</i>	<i>DCTD, WWC2, C4orf38</i>

exhibit major (CFH region at 1q32 and ARMS2 region at 10q26) or minor (C2/CFB, C3, CFI, ABCA4) contributions to AMD susceptibility (66). A number of additional loci were recently suggested to exhibit significant genetic association in a GWAS (25); however, their relevance to AMD would require functional validation. Our cross-sectional analysis that examined SNPs near the 154 RPE signature genes for association in the AMD-GWAS data set revealed four genes, including *TIMP3*. We also identified three additional genes such as *CHRNA3*, *GRAMD3* and *PITPNA* that deserve further investigations for their potential role in AMD etiology. *CHRNA3* encodes the nicotinic cholinergic receptor alpha 3, a

member of the nicotinic acetylcholine receptor family, which plays an important role in calcium regulation, neuronal development and cognitive functions (67,68). Mutations in this gene lead to dysfunction associated with various neurodegenerative disorders, including Alzheimer's disease, Parkinson's, epilepsy and autism. In RPE, deregulation of Ca^{2+} signaling could significantly impair overall cell physiology, for example, leading to abnormal fluid absorption, or to the abnormal secretion of different growth factors, including VEGF, leading to the development of neovascular AMD (69,70).

Further bioinformatic analysis (71) of the 48 RPE signature genes that showed nominal association with AMD revealed

	N-region	H-core	C-region	Peptide Length	%Hydrophobic residues per whole peptide
PDPN		<u>MW</u> <u>KV</u> <u>SALL</u> <u>FL</u> <u>VL</u> <u>GSASL</u> <u>WV</u> <u>LAEG</u>		22	59
DCT		<u>MS</u> <u>PL</u> <u>WGF</u> <u>LL</u> <u>SCL</u> <u>GCK</u> <u>IL</u> <u>PQA</u> <u>QG</u>		23	52
SDC2		<u>MRR</u> <u>AW</u> <u>ILL</u> <u>TL</u> <u>GL</u> <u>VAC</u> <u>VSA</u>		18	61
GNMB		<u>ME</u> <u>CL</u> <u>YY</u> <u>FL</u> <u>GF</u> <u>LL</u> <u>LA</u> <u>RL</u> <u>PL</u> <u>DA</u>		21	71
ASAH1		<u>MP</u> <u>GR</u> <u>SC</u> <u>VAL</u> <u>VLL</u> <u>AAV</u> <u>SC</u> <u>AVA</u>		21	71
TIMP3		<u>MT</u> <u>PWL</u> <u>GL</u> <u>I</u> <u>VLL</u> <u>GS</u> <u>W</u> <u>SL</u> <u>GD</u> <u>WG</u> <u>AEA</u>		23	57
CALU		<u>MD</u> <u>L</u> <u>RQ</u> <u>FL</u> <u>M</u> <u>C</u> <u>L</u> <u>S</u> <u>L</u> <u>C</u> <u>T</u> <u>A</u> <u>F</u> <u>A</u> <u>L</u> <u>S</u>		19	53
SOSD1		<u>ML</u> <u>P</u> <u>PA</u> <u>I</u> <u>H</u> <u>F</u> <u>Y</u> <u>L</u> <u>L</u> <u>P</u> <u>L</u> <u>A</u> <u>C</u> <u>I</u> <u>L</u> <u>M</u> <u>K</u> <u>S</u> <u>C</u> <u>L</u> <u>A</u>		23	82
OSTM1		<u>ME</u> <u>P</u> <u>G</u> <u>P</u> <u>T</u> <u>A</u> <u>A</u> <u>Q</u> <u>R</u> <u>R</u> <u>C</u> <u>S</u> <u>L</u> <u>P</u> <u>P</u> <u>W</u> <u>L</u> <u>P</u> <u>L</u> <u>G</u> <u>L</u> <u>L</u> <u>L</u> <u>S</u> <u>G</u> <u>L</u> <u>A</u> <u>L</u> <u>G</u>		31	61
VEGF		<u>MN</u> <u>F</u> <u>L</u> <u>L</u> <u>S</u> <u>W</u> <u>V</u> <u>H</u> <u>S</u> <u>L</u> <u>A</u> <u>L</u> <u>L</u> <u>L</u> <u>L</u> <u>L</u> <u>L</u> <u>L</u> <u>H</u> <u>H</u> <u>A</u> <u>K</u> <u>W</u> <u>S</u> <u>Q</u> <u>A</u>		26	58
TFPI2		<u>MD</u> <u>P</u> <u>A</u> <u>R</u> <u>P</u> <u>L</u> <u>G</u> <u>L</u> <u>S</u> <u>I</u> <u>L</u> <u>L</u> <u>L</u> <u>F</u> <u>L</u> <u>T</u> <u>E</u> <u>A</u> <u>A</u> <u>L</u> <u>G</u>		22	64
PRNP		<u>MA</u> <u>N</u> <u>L</u> <u>G</u> <u>C</u> <u>W</u> <u>M</u> <u>L</u> <u>V</u> <u>L</u> <u>F</u> <u>V</u> <u>A</u> <u>T</u> <u>W</u> <u>S</u> <u>D</u> <u>L</u> <u>G</u> <u>L</u> <u>C</u>		22	59
CHRNA3	<u>MAL</u> <u>AV</u> <u>S</u> <u>L</u> <u>P</u> <u>L</u> <u>A</u> <u>L</u> <u>S</u> <u>P</u> <u>P</u> <u>R</u> <u>L</u> <u>L</u> <u>L</u> <u>L</u> <u>L</u> <u>S</u> <u>L</u> <u>L</u> <u>P</u> <u>V</u> <u>A</u> <u>R</u> <u>A</u>			29	79
SERPINF1		<u>MQ</u> <u>AL</u> <u>V</u> <u>L</u> <u>L</u> <u>L</u> <u>C</u> <u>I</u> <u>G</u> <u>A</u> <u>L</u> <u>L</u> <u>G</u> <u>H</u> <u>S</u> <u>S</u> <u>C</u>		19	57
SILV		<u>MD</u> <u>L</u> <u>V</u> <u>L</u> <u>K</u> <u>R</u> <u>C</u> <u>L</u> <u>L</u> <u>H</u> <u>L</u> <u>A</u> <u>V</u> <u>I</u> <u>G</u> <u>A</u> <u>L</u> <u>L</u> <u>A</u> <u>V</u> <u>G</u> <u>A</u> <u>T</u>		24	63
ADAM9	<u>MG</u> <u>S</u> <u>G</u> <u>A</u> <u>R</u> <u>F</u> <u>P</u> <u>S</u> <u>G</u> <u>T</u> <u>L</u> <u>R</u> <u>V</u> <u>R</u> <u>W</u> <u>L</u> <u>L</u> <u>L</u> <u>L</u> <u>G</u> <u>L</u> <u>V</u> <u>G</u> <u>P</u> <u>V</u> <u>L</u> <u>G</u>			28	54
PCYOX1		<u>M</u> <u>G</u> <u>R</u> <u>V</u> <u>A</u> <u>E</u> <u>L</u> <u>V</u> <u>S</u> <u>S</u> <u>L</u> <u>L</u> <u>G</u> <u>L</u> <u>W</u> <u>L</u> <u>L</u> <u>L</u> <u>C</u> <u>S</u> <u>C</u> <u>G</u> <u>C</u> <u>P</u> <u>E</u> <u>G</u>		27	48
PTPRG		<u>M</u> <u>R</u> <u>R</u> <u>L</u> <u>L</u> <u>E</u> <u>P</u> <u>C</u> <u>W</u> <u>W</u> <u>I</u> <u>L</u> <u>F</u> <u>L</u> <u>K</u> <u>I</u> <u>T</u> <u>S</u> <u>P</u> <u>T</u> <u>P</u> <u>R</u>		22	59

- Green: hydrophilic N-region (N-terminus of the peptide)
- Red: hydrophobic core (H-core) common for all signal peptides
- Blue: flanking C-terminal region located next to coding region
- Underlined residues predicted to form helices

Figure 8. Structure of signal peptides and protein localization for 18 proteins obtained as the result of cross validation between GWAS and RPE signature studies. All of the presented peptides have a tripartite structure consisting of a central hydrophobic region (H-core, red), N-terminal hydrophilic region (N-region, green) and C-terminal flanking region located next to the protein (C-region, blue). Residues predicted to form α -helices are underlined. The H-core is helical in a majority of sequences and formed by leucine, alanine and valine residues. Protein localization was obtained using the UniProt information resource (<http://pir.georgetown.edu>) and sequences were aligned using the Promals3D program (<http://prodata.swmed.edu/promals3d/promals3d.php>).

similar signal peptide sequences in 18 of the encoded proteins (Fig. 8; 72–74). There is growing evidence that signal peptides play a major role in controlling protein sorting and trafficking in the endoplasmic reticulum [ER (75–77)]. Accumulation of mild folding variants of the proteins due to polymorphic variations/mutations leads to the aggregation of misfolded proteins, increased ER stress and eventual cell degeneration. For example, late-onset autosomal dominant retinal macular degeneration (L-ORMD), which phenotypically resembles AMD, is caused by mutations in *C1QTNF5*, a short-chain collagen gene expressed in the RPE. It has been proposed that mutant CTRP5 is misfolded, retained in the ER and subjected to degradation leading to RPE dysfunction (78). The phenotype of L-ORMD is similar to Sorsby's fundus dystrophy caused by mutations in *TIMP3*. In both cases, ER stress and abnormal cell adhesion cause cell degeneration and a failure to clear cellular debris from under the RPE, which suggests the possibility of immune attack—as seen in AMD (79).

As RPE is thought to be a critical target for AMD, numerous investigations have focused on regenerating or replacing damaged RPE from ES cells or from iPS cells. Several human ES lines can be induced to develop the RPE phenotype (80–82) and one of these has been used in transplantation experiments to rescue visual function in RCS rats (83). However, in the absence of a molecular signature, it is difficult to assess which *in vitro* generated RPE lines will retain appropriate function after transplantation. The RPE signature gene set can therefore be a valuable tool in regenerative medicine for validating the progress of RPE differentiation, propagation and maintenance. For clinical trials, it would be critical to confirm that RPE cell lines derived from hES cells exhibit

an expression profile comparable with the native RPE. We suggest that the signature gene set can be used to monitor the development to RPE phenotype and, together with functional tests such as polarity and physiology (18,84), can determine appropriate cell lines for transplantation and rescue experiments.

In conclusion, we have described a specific gene signature of human RPE based on extensive analysis of native and cultured cells. Our analysis of the 154 RPE signature gene set provides a wealth of information for biological studies, reveals candidate genes for retinal/macular diseases and suggests potential molecular markers for assessing the integrity and function of RPE for cell-based therapies.

MATERIALS AND METHODS

Native tissues and cell culture

This research followed the tenets of the Declaration of Helsinki and the guidelines of NIH Institutional Review Board and written informed consent was obtained from the GWAS subjects. Human fetal eyes (gestation, 16–18 weeks) were obtained from Advanced Bioscience Resources (Alameda, CA, USA) and human adult eyes were obtained from Analytical Biological Services, Inc. (Wilmington, DE, USA). Human adult native RPE (anRPE) were obtained from four donors of Caucasian descent (age 64–89 years old) within 24 h of death (postmortem time <12 h). Human fetal native RPE (fnRPE), retina and human fetal choroid (hfCH) were isolated and fnRPE were cultured on Primaria[®] flasks as described previously (18). For immunofluorescence localization or fluid transport experiments, cells were cultured on human ECM-

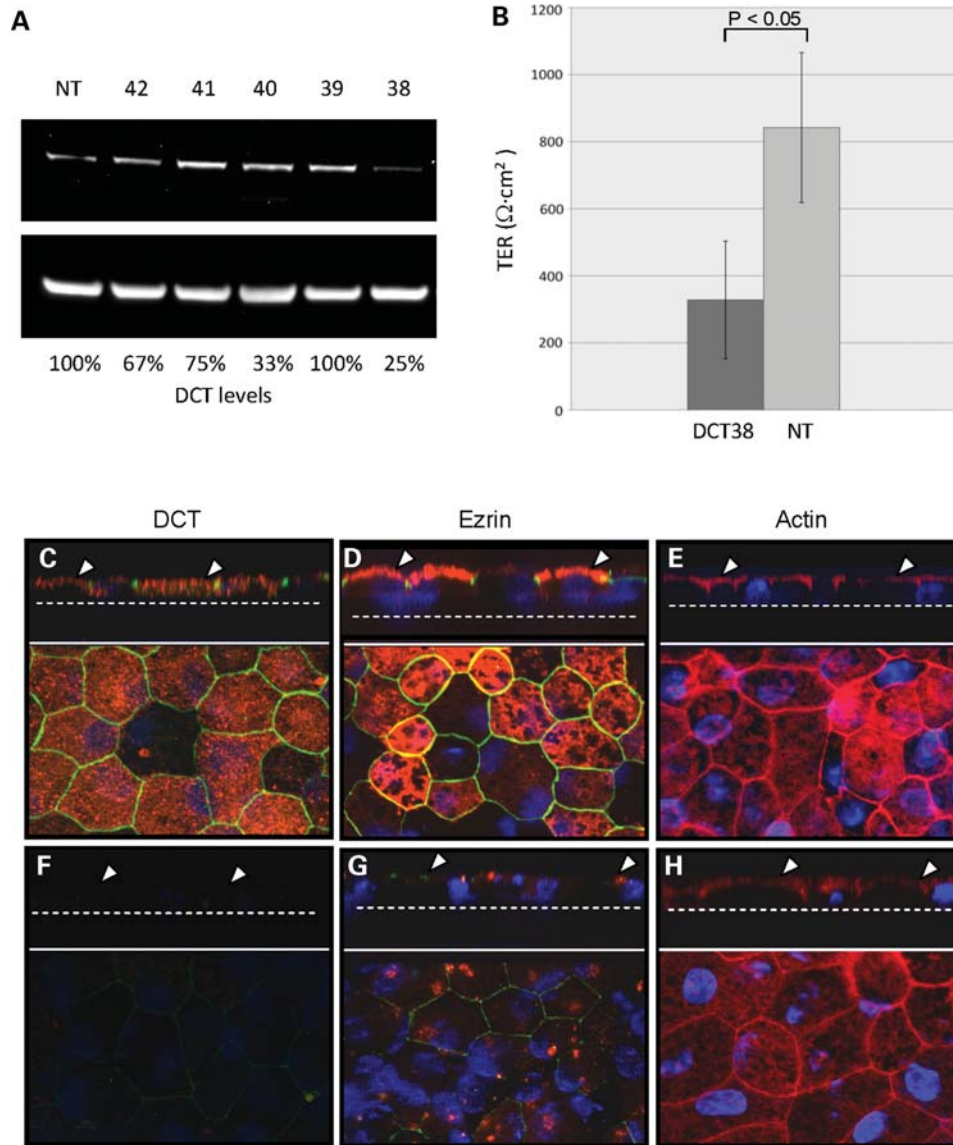


Figure 9. DCT silencing in hfrPE cultures grown on cell culture inserts using lentiviral-mediated transduction of shRNA. **(A)** Semi-quantitative evaluation of western blots of DCT after transduction with different shRNA clones. Labels indicate different clones: NT—non-targeting construct and 38–42 are DCT targeting shRNA clones. After quantification of band intensities and normalization to tubulin, DCT protein expression shRNA transduced cells were calculated relative to that of the cells transduced with NT shRNA (100%). **(B)** Transepithelial resistance measurements of confluent hfrPE monolayers grown on inserts transduced with DCT38 shRNA clones and compared with an NT construct controls ($P < 0.05$; $n = 6$). **(C–H)** Representative immunohistochemistry staining of hfrPE cells expressing shRNA directed against DCT (F, G, and H) and NT control shRNA (C, D, and E). Lower part of each panel is an *en face* view of maximum intensity projection (MIP) through the *z*-axis. Top part of each panel is a cross-sectional view through the *z*-plane. Lowest part of DAPI signal (dotted white lines) delineates the basal membrane. White arrowheads point to hfrPE apical surface. Red: DCT (C, F), ezrin (D, G), actin (E, H). Blue: DAPI-stained nuclei; green: ZO-1 indicates tight junction location separating apical and basolateral membranes. Transduction of hfrPE cells with DCT38 shRNA dramatically reduced the DCT levels inside cells (F), reduced and disorganized ZO-1 localization (F and G), and disrupted F-actin fibers to a more diffuse pattern with apical localization (H).

coated transwells (Corning Costar, 0.4 μm pores, polyester membrane). ARPE-19, a spontaneously transformed RPE cell line, was maintained under culturing conditions identical to fetal RPE primary cultures. The initial experimental design included separate samples of RPE grown on flasks (passage P_0) or inserts (passage P_1) coated with ECM. As no significant difference was observed between expression profiles of the cells grown on flasks or inserts (data not shown), we merged the two data sets for subsequent analysis.

Protein analysis

RPE, retina or choroid cells were lysed in RIPA buffer (Sigma-Aldrich, St. Louis, MO, USA) containing a proteinase inhibitor cocktail (Roche, Indianapolis, IN, USA). Protein extracts (10–15 μg) were electrophoresed using 4–12% Bis-Tris NuPAGE gel and blotted onto nitrocellulose membranes (Invitrogen, Carlsbad, CA, USA). The blots were incubated with antibodies against human BEST1, TYRP1 (Abcam,

Table 3. Twenty-five candidate RPE signature genes found in loci associated with retinal disease

Disease locus ^a	Disease name	Chromosomal location ^b	Candidate RPE genes
LCA9	Recessive Leber congenital amaurosis	1p36	<i>PDPN, KLHL21</i>
CORD8	Recessive cone-rod dystrophy	1q23.1–q23.3	<i>BAT2D1</i>
RP28	Recessive retinitis pigmentosa	2p16–p11	<i>USP34</i>
CRV,HERNS,HVR	Dominant hereditary vascular retinopathy	3p21.3–p21.1	<i>CSPG5,SLC6A20,PTPRG</i>
MCDR3	Dominant macular dystrophy	5p15.33–p13.1	<i>SCAMP1,RHOBTB3</i>
BCMAD	Dominant macular dystrophy	6p12.3–q16	<i>EFHC1, VEGFA</i>
MDDC	Dominant macular dystrophy, cystoid	7p21–p15	<i>SOSTDC1,SEMA3C</i>
OPA6, ROA1	recessive optic atrophy	8q21–q22	<i>LAPTM4B,SDC2</i>
EVR3	Dominant familial exudative vitreoretinopathy	11p13–p12	<i>FADS1</i>
CODA1	Dominant cavitory optic disc anomalies	12q13.13–q14.3	<i>ATF,SILV,NAV3</i>
MRST	Retinal degeneration, retardation	15q24	<i>CHRNA3</i>
OPA4	Dominant optic atrophy	18q12.2–q12.3	<i>SLC39A6</i>
MCDR5	Dominant macular dystrophy	19q13.31–q13.32	<i>CRX</i>
RP23	X-linked retinitis pigmentosa	Xp22	<i>GPM6B,CLCN4, GPR143</i>

^aInformation about disease loci collected from RetNet: www.sph.uth.tmc.edu/retnet/

^bChromosome location of disease loci.

Cambridge, MA, USA), CDH3 (Invitrogen), RPE65 (Dr. T. M. Redmond, NEI, NIH), CHRNA3 (Proteintech group, Inc., Chicago, IL, USA), or CRX (Abnova, Walnut, CA, USA). β -Actin and α -tubulin (Abcam) were used as controls. Immunoblot signals were detected using West Dura Chemiluminescence system (Pierce), imaged using Autochemie™ system (UVP, Upland, CA, USA), and quantified using Labworks software.

Immunocytochemistry

hfRPE cultures on cell culture inserts (Transwell; Corning Costar) transduced with MISSION lentiviral particles were fixed for 30 min in 4% formaldehyde–PBS on ice, washed three times with PBS, and permeabilized for 30 min with 0.2% Triton X-100–PBS. The cells were washed three times with PBS, stained with antibodies against DCT (1:1000, ProteinTech), ezrin (1:500, Abcam), ZO-1 (1:1500, Invitrogen) overnight at 4°C in blocking solution, following by incubated with Alexa Fluor conjugated secondary antibodies (1:1000, Invitrogen) for 2 h and mounting with Vectashield medium containing DAPI (VectorLabs). F-actin was stained with Texas Red phalloidin (Molecular Probes). Stained inserts were imaged for microscopy (Axioplan 2 with Axiovision 3.4 software with ApoTome; Carl Zeiss Meditec, Inc., Dublin, CA, USA). Negative controls were performed with omission of primary antibodies.

Lentivirus transduction

Lentiviruses have the unique ability to infect nondividing cells. MISSION™ (Sigma) lentiviral system was used to deliver specific short-hairpin RNAs (shRNA) in hfRPE cells to mediate the levels of DCT expression. Target hfRPE cells were seeded in a 24-well insert (2×10^5 /well), grown to confluence and cultured for 4–6 weeks. Hexadimethrine bromide (8 μ g/ml) was added to increase the efficiency of lentiviral transduction (Sigma), and all the transductions were performed at minimum effective multiplicity of infection of 2. The use of lentivirus shRNA resulted in 98% transduction efficiency. Viral medium was removed after 24 h of transduction and DCT protein levels were measure by western blots a week later. Immunocytochem-

istry staining was performed 3 weeks after the transduction. The functional effects on intact monolayers were evaluated by measurement of TER using EVOM (Precision Instruments).

RNA profiling

RNA was extracted from human tissues and cells using RNeasy Kit (Qiagen, Valencia, CA, USA) or total RNA isolation kit (Superarray Biosciences, Frederick, MD, USA). The panel of human tissues and cell cultures in this study included brain, melanocytes, colon, intestine, kidney, lung, trachea, testes, liver, calu-3 cells and a tissue mix, and were obtained commercially (Ambion First Choice Survey). Concentration and quality of RNA was determined using Bioanalyzer (Agilent Technologies, Palo Alto, CA, USA) and/or Nano drop spectrophotometer (Wilmington, DE, USA). All samples had A(260)/A(280) ratios of the total RNA >2.0, and the ratio of 28S/18S ribosomal RNA bands was more than 1.8. The purity of RPE preparations was confirmed by measuring transcript levels of rhodopsin. We also confirmed the absence of several choroid-specific transcripts (*S100A4, RGS5, ACTA2, ACTN1*) in RPE samples. The absence of cross-contamination was confirmed in retina and choroid samples from the same eye by measuring *RPE65* transcript levels. For the RNA Affymetrix chip analysis, we used The Vanderbilt Functional Genomics Shared Resource (FGSR). For each sample, the RNA integrity was indicated by an RIN number ranging from 0 to 10, with higher numbers indicating higher quality and we used samples with RIN >7. All four RPE groups (FC, AC, FN and AN) were definitively distinguished by the microarray analysis. Supplementary Material, Figure S1 shows that the RPE tissues are relatively indistinguishable from each other, but most importantly they are all clearly segregated from the other tissue types throughout the body. The relative uniformity of mean gene expression, from tissue to tissue, and their low variance indicates that the data are not limited by relatively small sample size.

The cDNA, reverse-transcribed from total RNA, was used to generate biotinylated cRNA with a BioArray High Yield RNA Transcript Labeling Kit (Affymetrix, Santa Clara, CA, USA). Fifteen micrograms of fragmented cRNA were hybri-

dized to expression microarrays (human GeneChips U133A plus 2.0 array, Affymetrix).

The signal intensity for each of 54 675 probe sets on the Affymetrix Human U133 plus 2.0 chips was calculated using GeneChip® Operating Software 1.4 (Affymetrix). Affymetrix probe set signal intensities were median normalized, i.e. divided by the median of each chip, and log₁₀ transformed. Normalization and statistical analysis were carried out using the MSCL Analysts Toolbox (<http://abs.cit.nih.gov/MSCLtoolbox/>), a microarray analysis package that consists of custom-written scripts in the JMP statistical discovery software (SAS Institute, Cary, NC, USA), and developed by two of the co-authors (P.J.M., J.J.B.). Data were collected under the MIAME compliant format and the raw data have been deposited in the Gene Expression Omnibus hosted by NCBI (GEO; <http://www.ncbi.nlm.nih.gov/geo/query/>) with query accession no: GSE18811. Visualization of the global relationships among the 30 samples and detection of possible outliers were facilitated with PCA biplots of the normalized data (85). Hierarchical clustering of the 30 samples, using all principal components and Ward's method, produces a dendrogram and an ordering of samples into clusters.

Validation of expression data by qRT-PCR

Quantitative mRNA analysis was performed for 150 genes using RT two real-time pre-developed primer sets (SuperArray, Frederick, MD, USA). Relative changes in gene expression were calculated using a variation of the $\Delta\Delta C_t$ method. The ΔC_t is the threshold cycle of the gene Ct value (copies $\times 10^5/\mu\text{g}$ RNA) minus the average of the Ct values of five housekeeping genes (B2M, HPRT1, RPL13A, GAPDH and ACTB). The average ΔC_t was calculated for each individual group (fc, fn, ac, an) of RPE tissues and for each of the comparison tissues. There were at least two biological replicates in each group of RPE tissue.

Derivation of RPE 'gene signature'

Highly expressed RPE probe sets were identified in terms of rEx level, rEx (86). The rEx for an RPE tissue is defined as the ratio of RPE expression to the median expression of 78 diverse anatomical samples (Genomics Institute of Novartis Research Foundation tissue data set). This set was augmented with several additional tissues of local origin (<http://biogps.gnf.org/#goto=welcome>). Both the RPE and the Novartis data were normalized using the log-median transformation. Since the Novartis data were collected on older Affymetrix U133A GeneChip, it had only ~40% of the number of probe sets in the newer U133 Plus 2 chip used for the RPE data. A gene is included as an RPE signature gene if its mean expression level in all three tissues, native adult and fetal RPE and cultured fetal RPE, are 10-fold or greater than the median expression for that gene in the Novartis data set. Each signature gene can have multiple probe sets in the RPE signature set.

GO analysis

Functional annotation, classification and identification of significantly enriched biological themes of RPE signature genes

were examined using The Database for Annotation, Visualization and Integrated Discovery (71) bioinformatics resource (<http://david.abcc.ncifcrf.gov/>) and Expression Analysis Systematic Explorer (EASE) (<http://apps1.niaid.nih.gov/david>). GO terminology for 'biological processes' (<http://www.geneontology.org/>) was used to identify significant overrepresentation of functional classes in the RPE signature list, as described previously (87,88). EASE score or Fisher's exact test *P*-value was used to measure the significance of the gene-enrichment within each biological process category.

Comparison of RPE genes to AMD–GWAS data

To examine possible association of RPE 'signature' genes to AMD, we identified SNPs within 100 kb of the 5' and 3' ends of the RPE 'signature' genes and evaluated their association with macular degeneration in a recently completed AMD–GWAS (89). The GWAS data included 2157 AMD cases and 1150 controls, each examined on 324 067 SNPs using Illumina Human 370CNV BeadChips. An additional ~2.2 million markers arrays were imputed using HapMap genotypes and were also examined (90). A total of 33 096 SNPs near 154 RPE signature genes were examined, corresponding to a Bonferroni significance threshold of 1.5×10^{-6} . The 33 096 correspond to 4305 independent tag SNPs. To identify additional SNPs that may be implicated in AMD pathogenesis, we also evaluated false discovery rates (91) and inspected quantile–quantile plots for all SNPs.

eQTL analysis

A database of expression quantitative trait loci, obtained by GWA analysis of SNPs with gene expression levels in lymphoblastoid cell lines (30), was searched for regulatory SNPs associated with RPE 'signature' genes. The evidence for association between each of these potential regulatory SNPs and AMD was then evaluated based on the data of Chen *et al.* (25). The Dixon *et al.* data consist of a catalog of association between SNPs and transcripts generated by examining lymphoblastoid cell lines from ~400 children.

SUPPLEMENTARY MATERIAL

Supplementary Material is available at *HMG* online.

ACKNOWLEDGEMENTS

We are pleased to thank Jing Zhao, Connie Zhang, and Awais Zia for technical assistance. We also thank Ramanujan Hegde (NICHD/NIH) for helpful discussion of protein signal sequences.

Conflict of Interest statement. None declared.

FUNDING

This research was supported by the Intramural and Extramural Research Programs of the National Eye Institute, NIH. Funding to pay the Open Access publication charges for this article was provided by NIH Intramural Program.

REFERENCES

- Rein, D.B., Wittenborn, J.S., Zhang, X., Honeycutt, A.A., Lesesne, S.B. and Saaddine, J. (2009) Forecasting age-related macular degeneration through the year 2050: the potential impact of new treatments. *Arch. Ophthalmol.*, **127**, 533–540.
- Krishnan, T., Ravindran, R.D., Murthy, G.V., Vashist, P., Fitzpatrick, K.E., Thulasiraj, R.D., John, N., Maraini, G., Camparini, M., Chakravarthy, U. *et al.* (2009) Prevalence of early and late age-related macular degeneration in India: the INDEYE study. *Invest. Ophthalmol. Vis. Sci.*, **51**, 701–707.
- Swaroop, A., Chew, E.Y., Rickman, C.B. and Abecasis, G.R. (2009) Unraveling a multifactorial late-onset disease: from genetic susceptibility to disease mechanisms for age-related macular degeneration. *Annu. Rev. Genomics Hum. Genet.*, **10**, 19–43.
- Cai, X., Conley, S.M. and Naash, M.I. (2009) RPE65: role in the visual cycle, human retinal disease, and gene therapy. *Ophthalmic Genet.*, **30**, 57–62.
- Nussenblatt, R.B. and Ferris, F. 3rd (2007) Age-related macular degeneration and the immune response: implications for therapy. *Am. J. Ophthalmol.*, **144**, 618–626.
- Wang, Q., Chen, Q., Zhao, K., Wang, L., Wang, L. and Traboulsi, E.I. (2001) Update on the molecular genetics of retinitis pigmentosa. *Ophthalmic Genet.*, **22**, 133–154.
- Hughes, B.A., Gallemore, R.P. and Miller, S.S. (1998) Transport mechanisms in the retinal pigment epithelium. In Marmor, M.F. and Wolfensberger, T.J. (eds), *The Retinal Pigment Epithelium*, Oxford University Press, New York, pp. 103–134.
- Strauss, O. (2005) The retinal pigment epithelium in visual function. *Physiol. Rev.*, **85**, 845–881.
- Maeda, A., Maeda, T., Golczak, M. and Palczewski, K. (2008) Retinopathy in mice induced by disrupted all-trans-retinal clearance. *J. Biol. Chem.*, **283**, 26684–26693.
- Adijanto, J., Banzon, T., Jalickee, S., Wang, N.S. and Miller, S.S. (2009) CO₂-induced ion and fluid transport in human retinal pigment epithelium. *J. Gen. Physiol.*, **133**, 603–622.
- Vives-Bauza, C., Anand, M., Shirazi, A.K., Magrane, J., Gao, J., Vollmer-Snarr, H.R., Manfredi, G. and Finnemann, S.C. (2008) The age lipid A2E and mitochondrial dysfunction synergistically impair phagocytosis by retinal pigment epithelial cells. *J. Biol. Chem.*, **283**, 24770–24780.
- Tian, J., Ishibashi, K. and Handa, J.T. (2004) The expression of native and cultured RPE grown on different matrices. *Physiol. Genomics*, **17**, 170–182.
- Buraczynska, M., Mears, A.J., Zarepari, S., Farjo, R., Filippova, E., Yuan, Y., MacNee, S.P., Hughes, B. and Swaroop, A. (2002) Gene expression profile of native human retinal pigment epithelium. *Invest. Ophthalmol. Vis. Sci.*, **43**, 603–607.
- Dunn, K.C., Aotaki-Keen, A.E., Putkey, F.R. and Hjelmeland, L.M. (1996) ARPE-19, a human retinal pigment epithelial cell line with differentiated properties. *Exp. Eye Res.*, **62**, 155–169.
- Gamm, D.M., Melvan, J.N., Shearer, R.L., Pinilla, I., Sabat, G., Svendsen, C.N. and Wright, L.S. (2008) A novel serum-free method for culturing human prenatal retinal pigment epithelial cells. *Invest. Ophthalmol. Vis. Sci.*, **49**, 788–799.
- Ishida, M., Lui, G.M., Yamani, A., Sugino, I.K. and Zarbin, M.A. (1998) Culture of human retinal pigment epithelial cells from peripheral scleral flap biopsies. *Curr. Eye Res.*, **17**, 392–402.
- da Cruz, L., Chen, F.K., Ahmado, A., Greenwood, J. and Coffey, P. (2007) RPE transplantation and its role in retinal disease. *Prog. Retin. Eye Res.*, **26**, 598–635.
- Maminishkis, A., Chen, S., Jalickee, S., Banzon, T., Shi, G., Wang, F.E., Ehalt, T., Hammer, J.A. and Miller, S.S. (2006) Confluent monolayers of cultured human fetal retinal pigment epithelium exhibit morphology and physiology of native tissue. *Invest. Ophthalmol. Vis. Sci.*, **47**, 3612–3624.
- Klimanskaya, I., Rosenthal, N. and Lanza, R. (2008) Derive and conquer: sourcing and differentiating stem cells for therapeutic applications. *Nat. Rev. Drug Discov.*, **7**, 131–142.
- Hu, J. and Bok, D. (2001) A cell culture medium that supports the differentiation of human retinal pigment epithelium into functionally polarized monolayers. *Mol. Vis.*, **7**, 14–19.
- Quinn, R.H. and Miller, S.S. (1992) Ion transport mechanisms in native human retinal pigment epithelium. *Invest. Ophthalmol. Vis. Sci.*, **33**, 3513–3527.
- Blaug, S., Quinn, R., Quong, J., Jalickee, S. and Miller, S.S. (2003) Retinal pigment epithelial function: a role for CFTR? *Doc. Ophthalmol.*, **106**, 43–50.
- Lin, H., Kenyon, E. and Miller, S.S. (1992) Na-dependent pHi regulatory mechanisms in native human retinal pigment epithelium. *Invest. Ophthalmol. Vis. Sci.*, **33**, 3528–3538.
- Booij, J.C., van Soest, S., Swagemakers, S.M., Essing, A.H., Verkerk, A.J., van der Spek, P.J., Gorgels, T.G. and Bergen, A.A. (2009) Functional annotation of the human retinal pigment epithelium transcriptome. *BMC Genomics*, **10**, 164–178.
- Chen, W., Stambolian, D., Edwards, A.O., Branham, K.E., Othman, M., Jakobsdottir, J., Tosakulwong, N., Pericak-Vance, M.A., Campochiaro, P.A., Klein, M.L. *et al.* (2010) Genetic variants near TIMP3 and HDL-associated loci influence susceptibility to age-related macular degeneration. *Proc. Natl Acad. Sci. USA*. (in press). Epub ahead of print April 12, 2010.
- Su, A.I., Wiltshire, T., Batalov, S., Lapp, H., Ching, K.A., Block, D., Zhang, J., Soden, R., Hayakawa, M., Kreiman, G. *et al.* (2004) A gene atlas of the mouse and human protein-encoding transcriptomes. *Proc. Natl Acad. Sci. USA*, **101**, 6062–6067.
- Johnson, L.V., Ozaki, S., Staples, M.K., Erickson, P.A. and Anderson, D.H. (2000) A potential role for immune complex pathogenesis in drusen degeneration. *Exp. Eye Res.*, **70**, 441–449.
- Chen, H., Lukas, T.J., Du, N., Suyeoka, G. and Neufeld, A.H. (2009) Dysfunction of the retinal pigment epithelium with age: increased iron decreases phagocytosis and lysosomal activity. *Invest. Ophthalmol. Vis. Sci.*, **50**, 1895–1902.
- Huang da, W., Sherman, B.T., Tan, Q., Kir, J., Liu, D., Bryant, D., Guo, Y., Stephens, R., Baseler, M.W., Lane, H.C. *et al.* (2007) DAVID bioinformatics resources: expanded annotation database and novel algorithms to better extract biology from large gene lists. *Nucleic Acids Res.*, **35**, 169–175.
- Dixon, A.L., Liang, L., Moffatt, M.F., Chen, W., Heath, S., Wong, K.C., Taylor, J., Burnett, E., Gut, I., Farrall, M. *et al.* (2007) A genome-wide association study of global gene expression. *Nat. Genet.*, **39**, 1202–1207.
- Tsukamoto, K., Jackson, I.J., Urabe, K., Montague, P.M. and Hearing, V.J. (1992) A second tyrosinase-related protein, TRP-2, is a melanogenic enzyme termed DOPachrome tautomerase. *EMBO J.*, **11**, 519–526.
- Michard, Q., Commo, S., Rocchetti, J., El Houari, F., Alleaume, A.M., Wakamatsu, K., Ito, S. and Bernard, B.A. (2008) TRP-2 expression protects HEK cells from dopamine- and hydroquinone-induced toxicity. *Free Radic Biol. Med.*, **45**, 1002–1010.
- Bassi, M.T., Schiaffino, M.V., Renieri, A., De Nigris, F., Galli, L., Bruttini, M., Gebbia, M., Bergen, A.A., Lewis, R.A. and Ballabio, A. (1995) Cloning of the gene for ocular albinism type 1 from the distal short arm of the X chromosome. *Nat. Genet.*, **10**, 13–19.
- Lopez, V.M., Decatur, C.L., Stamer, W.D., Lynch, R.M. and McKay, B.S. (2008) L-DOPA is an endogenous ligand for OA1. *PLoS Biol.*, **6**, 236–247.
- Palmisano, I., Bagnato, P., Palmigiano, A., Innamorati, G., Rotondo, G., Altamare, D., Venturi, C., Sviderskaya, E.V., Piccirillo, R., Coppola, M. *et al.* (2008) The ocular albinism type 1 protein, an intracellular G protein-coupled receptor, regulates melanosome transport in pigment cells. *Hum. Mol. Genet.*, **17**, 3487–3501.
- Schlotzer-Schrehardt, U., Pasutto, F., Sommer, P., Hornstra, I., Kruse, F.E., Naumann, G.O., Reis, A. and Zenkel, M. (2008) Genotype-correlated expression of lysyl oxidase-like 1 in ocular tissues of patients with pseudoexfoliation syndrome/glaucoma and normal patients. *Am. J. Pathol.*, **173**, 1724–1735.
- Yu, H.G., Liu, X., Kiss, S., Connolly, E., Gragoudas, E.S., Michaud, N.A., Bulgakov, O.V., Adamian, M., DeAngelis, M.M., Miller, J.W. *et al.* (2008) Increased choroidal neovascularization following laser induction in mice lacking lysyl oxidase-like 1. *Invest. Ophthalmol. Vis. Sci.*, **49**, 2599–2605.
- Escher, P., Cottet, S., Aono, S., Oohira, A. and Schorderet, D.F. (2008) Differential neuroglycan C expression during retinal degeneration in Rpe65^{-/-} mice. *Mol. Vis.*, **14**, 2126–2135.
- Espinosa, E.J., Calero, M., Sridevi, K. and Pfeiffer, S.R. (2009) RhoBTB3: a Rho GTPase-family ATPase required for endosome to Golgi transport. *Cell*, **137**, 938–948.
- Liao, H., Zhang, J., Shestopal, S., Szabo, G., Castle, A. and Castle, D. (2008) Nonredundant function of secretory carrier membrane protein isoforms in dense core vesicle exocytosis. *Am. J. Physiol. Cell Physiol.*, **294**, 797–809.
- Banerjee, A.G., Bhattacharyya, I. and Vishwanatha, J.K. (2005) Identification of genes and molecular pathways involved in the progression of premalignant oral epithelia. *Mol. Cancer Ther.*, **4**, 865–875.

42. Takeda, K., Yokoyama, S., Aburatani, H., Masuda, T., Han, F., Yoshizawa, M., Yamaki, N., Yamamoto, H., Eguchi, N., Urade, Y. *et al.* (2006) Lipocalin-type prostaglandin D synthase as a melanocyte marker regulated by MITF. *Biochem. Biophys. Res. Commun.*, **339**, 1098–1106.
43. Huang, X., Xiao, D.W., Xu, L.Y., Zhong, H.J., Liao, L.D., Xie, Z.F. and Li, E.M. (2009) Prognostic significance of altered expression of SDC2 and CYR61 in esophageal squamous cell carcinoma. *Oncol. Rep.*, **21**, 1123–1129.
44. Munesh, S., Yoshitomi, Y., Kusano, Y., Koyama, Y., Nishiyama, A., Nakanishi, H., Miyazaki, K., Ishimaru, T., Miyaura, S., Okayama, M. *et al.* (2007) A novel function of syndecan-2, suppression of matrix metalloproteinase-2 activation, which causes suppression of metastasis. *J. Biol. Chem.*, **282**, 28164–28174.
45. Vormittag, L., Thurnher, D., Geleff, S., Pammer, J., Heiduschka, G., Brunner, M., Grasl, M. and Erovic, B.M. (2009) Co-expression of Bmi-1 and podoplanin predicts overall survival in patients with squamous cell carcinoma of the head and neck treated with radio(chemo)therapy. *Int. J. Radiat. Oncol. Biol. Phys.*, **73**, 913–918.
46. Yang, H.M., Cabral, E., Dadras, S.S. and Cassarino, D.S. (2008) Immunohistochemical expression of D2-40 in benign and malignant sebaceous tumors and comparison to basal and squamous cell carcinomas. *Am. J. Dermatopathol.*, **30**, 549–554.
47. Xie, Q., Chen, L., Fu, K., Harter, J., Young, K.H., Sunkara, J., Novak, D., Villanueva-Siles, E. and Ratche, H. (2008) Podoplanin (d2-40): a new immunohistochemical marker for reactive follicular dendritic cells and follicular dendritic cell sarcomas. *Int. J. Clin. Exp. Pathol.*, **1**, 276–284.
48. Parry, D.A., Toomes, C., Bida, L., Danciger, M., Towns, K.V., McKibbin, M., Jacobson, S.G., Logan, C.V., Ali, M., Bond, J. *et al.* (2009) Loss of the metalloprotease ADAM9 leads to cone-rod dystrophy in humans and retinal degeneration in mice. *Am. J. Hum. Genet.*, **84**, 683–691.
49. Chang, J.T., Esumi, N., Moore, K., Li, Y., Zhang, S., Chew, C., Goodman, B., Rattner, A., Moody, S., Stetten, G. *et al.* (1999) Cloning and characterization of a secreted frizzled-related protein that is expressed by the retinal pigment epithelium. *Hum. Mol. Genet.*, **8**, 575–583.
50. Garcia-Hoyos, M., Cantalapiedra, D., Arroyo, C., Esteve, P., Rodriguez, J., Riveiro, R., Trujillo, M.J., Ramos, C., Bovolenta, P. and Ayuso, C. (2004) Evaluation of SFRP1 as a candidate for human retinal dystrophies. *Mol. Vis.*, **10**, 426–431.
51. Tian, J., Ishibashi, K., Honda, S., Boylan, S.A., Hjelmeland, L.M. and Handa, J.T. (2005) The expression of native and cultured human retinal pigment epithelial cells grown in different culture conditions. *Br. J. Ophthalmol.*, **89**, 1510–1517.
52. Nevala, H., Ylikomi, T. and Tahti, H. (2008) Evaluation of the selected barrier properties of retinal pigment epithelial cell line ARPE-19 for an in-vitro blood-brain barrier model. *Hum. Exp. Toxicol.*, **27**, 741–749.
53. Hopfer, U., Fukai, N., Hopfer, H., Wolf, G., Joyce, N., Li, E. and Olsen, B.R. (2005) Targeted disruption of Col8a1 and Col8a2 genes in mice leads to anterior segment abnormalities in the eye. *FASEB J.*, **19**, 1232–1244.
54. Nordgaard, C.L., Berg, K.M., Kappahm, R.J., Reilly, C., Feng, X., Olsen, T.W. and Ferrington, D.A. (2006) Proteomics of the retinal pigment epithelium reveals altered protein expression at progressive stages of age-related macular degeneration. *Invest. Ophthalmol. Vis. Sci.*, **47**, 815–822.
55. Kim, J.W., Kang, K.H., Burrola, P., Mak, T.W. and Lemke, G. (2008) Retinal degeneration triggered by inactivation of PTEN in the retinal pigment epithelium. *Genes Dev.*, **22**, 3147–3157.
56. Calera, M.R., Topley, H.L., Liao, Y., Duling, B.R., Paul, D.L. and Goodenough, D.A. (2006) Connexin43 is required for production of the aqueous humor in the murine eye. *J. Cell. Sci.*, **119**, 4510–4519.
57. Schnetkamp, P.P. (2004) The SLC24 Na⁺/Ca²⁺-K⁺ exchanger family: vision and beyond. *Pflugers Arch.*, **447**, 683–688.
58. Everts, H.B., Sundberg, J.P., King, L.E. Jr and Ong, D.E. (2007) Immunolocalization of enzymes, binding proteins, and receptors sufficient for retinoic acid synthesis and signaling during the hair cycle. *J. Invest. Dermatol.*, **127**, 1593–1604.
59. Young, A., Powelson, E.B., Whitney, I.E., Raven, M.A., Nusinowitz, S., Jiang, M., Birnbaumer, L., Reese, B.E. and Farber, D.B. (2008) Involvement of OAI, an intracellular GPCR, and G alpha i3, its binding protein, in melanosomal biogenesis and optic pathway formation. *Invest. Ophthalmol. Vis. Sci.*, **49**, 3245–3252.
60. Gottsch, J.D., Sundin, O.H., Liu, S.H., Jun, A.S., Broman, K.W., Stark, W.J., Vito, E.C., Narang, A.K., Thompson, J.M. and Magovern, M. (2005) Inheritance of a novel COL8A2 mutation defines a distinct early-onset subtype of fuchs corneal dystrophy. *Invest. Ophthalmol. Vis. Sci.*, **46**, 1934–1939.
61. Takeda, K., Yokoyama, S., Yasumoto, K., Saito, H., Udono, T., Takahashi, K. and Shibahara, S. (2003) OTX2 regulates expression of DOPACHrome tautomerase in human retinal pigment epithelium. *Biochem. Biophys. Res. Commun.*, **300**, 908–914.
62. Jiao, Z., Zhang, Z.G., Hornyak, T.J., Hozeska, A., Zhang, R.L., Wang, Y., Wang, L., Roberts, C., Strickland, F.M. and Chopp, M. (2006) Dopachrome tautomerase (Dct) regulates neural progenitor cell proliferation. *Develop. Biol.*, **296**, 396–408.
63. Chu, W., Pak, B.J., Bani, M.R., Kapoor, M., Lu, S.J., Tamir, A., Kerbel, R.S. and Ben-David, Y. (2000) Tyrosinase-related protein 2 as a mediator of melanoma specific resistance to cis-diamminedichloroplatinum(II): therapeutic implications. *Oncogene*, **19**, 395–402.
64. Chen, K.G., Valencia, J.C., Gillet, J.P., Hearing, V.J. and Gottesman, M.M. (2009) Involvement of ABC transporters in melanogenesis and the development of multidrug resistance of melanoma. *Pigment Cell Melanoma Res.*, **22**, 740–749.
65. Wang, F.E., Zhang, C., Maminishkis, A., Dong, L., Zhi, C., Li, R., Zhao, J., Majerciak, V., Gaur, A.B., Chen, S. *et al.* (2010) MicroRNA-204/211 alters epithelial physiology. *FASEB J.*, [Epub ahead of print March 25, 2010].
66. Swaroop, A., Chew, E.Y., Bowes Rickman, C. and Abecasis, G.R. (2009) Unraveling a multifactorial late-onset disease: from genetic susceptibility to disease mechanisms for age-related macular degeneration. *Annu. Rev. Genomics Hum. Genet.*, **10**, 19–43.
67. Shen, J.X. and Yakel, J.L. (2009) Nicotinic acetylcholine receptor-mediated calcium signaling in the nervous system. *Acta Pharmacol. Sin.*, **30**, 673–680.
68. Lu, Y. and Wang, X. (2009) Genes associated with idiopathic epilepsies: a current overview. *Neurol. Res.*, **31**, 135–143.
69. Peterson, W.M., Meggyesy, C., Yu, K. and Miller, S.S. (1997) Extracellular ATP activates calcium signaling, ion, and fluid transport in retinal pigment epithelium. *J. Neurosci.*, **17**, 2324–2337.
70. Heesch, C., Weis, M., Aicher, A., Dimmeler, S. and Cooke, J.P. (2002) A novel angiogenic pathway mediated by non-neuronal nicotinic acetylcholine receptors. *J. Clin. Invest.*, **110**, 527–536.
71. Sternberg, P. Jr, Davidson, P.C., Jones, D.P., Hagen, T.M., Reed, R.L. and Drews-Botsch, C. (1993) Protection of retinal pigment epithelium from oxidative injury by glutathione and precursors. *Invest. Ophthalmol. Vis. Sci.*, **34**, 3661–3668.
72. Hegde, R.S. and Bernstein, H.D. (2006) The surprising complexity of signal sequences. *Trends Biochem. Sci.*, **31**, 563–571.
73. Kang, S.W. and Hegde, R.S. (2008) Lighting up the stressed ER. *Cell*, **135**, 787–789.
74. Martoglio, B. and Dobberstein, B. (1998) Signal sequences: more than just greasy peptides. *Trends Cell Biol.*, **8**, 410–415.
75. Mellman, I. and Nelson, W.J. (2008) Coordinated protein sorting, targeting and distribution in polarized cells. *Nat. Rev. Mol. Cell Biol.*, **9**, 833–845.
76. Hegde, R.S. and Kang, S.W. (2008) The concept of translocational regulation. *J. Cell Biol.*, **182**, 225–232.
77. Levine, C.G., Mitra, D., Sharma, A., Smith, C.L. and Hegde, R.S. (2005) The efficiency of protein compartmentalization into the secretory pathway. *Mol. Biol. Cell*, **16**, 279–291.
78. Shu, X., Tulloch, B., Lennon, A., Vlachantoni, D., Zhou, X., Hayward, C. and Wright, A.F. (2006) Disease mechanisms in late-onset retinal macular degeneration associated with mutation in C1QTNF5. *Hum. Mol. Genet.*, **15**, 1680–1689.
79. Qi, J.H., Ebrahem, Q., Yeow, K., Edwards, D.R., Fox, P.L. and Anand-Apte, B. (2002) Expression of Sorsby's fundus dystrophy mutations in human retinal pigment epithelial cells reduces matrix metalloproteinase inhibition and may promote angiogenesis. *J. Biol. Chem.*, **277**, 13394–13400.
80. Klimanskaya, I., Hipp, J., Rezaei, K.A., West, M., Atala, A. and Lanza, R. (2004) Derivation and comparative assessment of retinal pigment epithelium from human embryonic stem cells using transcriptomics. *Cloning Stem Cells*, **6**, 217–245.
81. Corneo, B. and Temple, S. (2009) Sense and serendipity aid RPE generation. *Cell Stem Cell*, **5**, 347–348.
82. Idelson, M., Alper, R., Obolensky, A., Ben-Shushan, E., Hemo, I., Yachimovich-Cohen, N., Khaner, H., Smith, Y., Wisner, O., Gropp, M. *et al.* (2009) Directed differentiation of human embryonic stem cells into functional retinal pigment epithelium cells. *Cell Stem Cell*, **5**, 396–408.
83. Vugler, A., Carr, A.J., Lawrence, J., Chen, L.L., Burrell, K., Wright, A., Lundh, P., Semo, M., Ahmado, A., Gias, C. *et al.* (2008) Elucidating the

- phenomenon of HESC-derived RPE: anatomy of cell genesis, expansion and retinal transplantation. *Exp. Neurol.*, **214**, 347–361.
84. Shi, G., Maminishkis, A., Banzon, T., Jalickee, S., Li, R., Hammer, J. and Miller, S.S. (2008) Control of chemokine gradients by the retinal pigment epithelium. *Invest. Ophthalmol. Vis. Sci.*, **49**, 4620–4630.
 85. Jolliffe, I.T. (2002) *Springer Series in Statistics: Principal Components Analysis*, Springer, New York, pp. 103–134.
 86. Bailey, M.J., Coon, S.L., Carter, D.A., Humphries, A., Kim, J.S., Shi, Q., Gaildrat, P., Morin, F., Ganguly, S., Hogenesch, J.B. *et al.* (2009) Night/day changes in pineal expression of >600 genes: central role of adrenergic/cAMP signaling. *J. Biol. Chem.*, **284**, 7606–7622.
 87. Dennis, G. Jr, Sherman, B.T., Hosack, D.A., Yang, J., Gao, W., Lane, H.C. and Lempicki, R.A. (2003) DAVID: database for annotation, visualization, and integrated discovery. *Genome Biol.*, **4**, 3.
 88. Hosack, D.A., Dennis, G. Jr, Sherman, B.T., Lane, H.C. and Lempicki, R.A. (2003) Identifying biological themes within lists of genes with EASE. *Genome Biol.*, **4**, R70.
 89. Carr, A.J., Vugler, A., Lawrence, J., Chen, L.L., Ahmado, A., Chen, F.K., Semo, M., Gias, C., da Cruz, L., Moore, H.D. *et al.* (2009) Molecular characterization and functional analysis of phagocytosis by human embryonic stem cell-derived RPE cells using a novel human retinal assay. *Mol. Vis.*, **15**, 283–295.
 90. Li, Y., Willer, C., Sanna, S. and Abecasis, G. (2009) Genotype imputation. *Annu. Rev. Genomics Hum. Genet.*, **10**, 387–406.
 91. Benjamini, Y. and Hochberg, Y. (1995) Controlling the false discovery rate: a practical and powerful approach to multiple testing. *J. R. Stat. Soc. B*, **57**, 289–300.